© 2020. Published by The Company of Biologists Ltd | Journal of Experimental Biology (2020) 223, jeb212928. doi:10.1242/jeb.212928

RESEARCH ARTICLE

Assessing intracellular pH regulation in H^+-ATPase-rich ionocytes in zebrafish larvae using *in vivo* ratiometric imaging

H. M. Yew, A. M. Zimmer and S. F. Perry*

ABSTRACT

The H^+-ATPase-rich (HR) cells of zebrafish larvae are a sub-type of ion-transporting cell located on the yolk sac epithelium that are responsible for Na^+ uptake and H^+ extrusion. Current models of HR cell ion transport mechanisms in zebrafish larvae are well established, but little is known about the involvement of the various ion transport pathways in regulating intracellular acid–base status. Here, a ratiometric imaging technique was developed and validated to monitor intracellular pH (pHi) continuously in larval zebrafish HR cells *in vivo*. Gene knockdown or CRISPR/Cas9 knockout approaches were used to evaluate the roles of the two principal apical membrane acid excretory pathways, the Na^+/H^+ exchanger (NHE3b; *slc9a3.2*) and the H^+-ATPase (*atpv1aa*). Additionally, the role of HR cell cytosolic carbonic anhydrase (CAc) was investigated because of its presumed role in providing H^+ for Na^+/H^+ exchange and H^+-ATPase. The temporal pattern and extent of intracellular acidification during exposure of fish to 1% CO_2 and the extent of post-CO_2 alkalisation were altered markedly in fish experiencing knockdown/knockout of CAc, NHE3b or H^+-ATPase. Although there were slight differences among the three knockdown/knockout experiments, the typical response was a greater degree of intracellular acidification during CO_2 exposure and a reduced capacity to restore pHi to baseline levels post-hypercapnia. The metabolic alkalosis and subsequent acidification associated with 20 mmol l^{-1} NH_4Cl exposure and its washout were largely unaffected by gene knockdown. Overall, the results suggest markedly different mechanisms of intracellular acid–base regulation in zebrafish HR cells depending on the nature of the acid–base disturbance.

KEY WORDS: Ionic regulation, Acid–base balance, Sodium–hydrogen exchanger (NHE), Carbonic anhydrase, *Danio rerio*, Morpholino knockdown, Ammonium chloride, Hypercapnia

INTRODUCTION

Freshwater fish possess effective osmoregulatory strategies to cope with the large ionic concentration differences between their body fluids and the external environment (reviewed by Evans et al., 2005; Marshall and Grosell, 2006; Hwang et al., 2011; Hiroi and McCormick, 2012). Specialised cells known as ionocytes or mitochondrion-rich (MR) cells express specific ion transport proteins enabling the active uptake of ions (i.e. Na^+, Cl^- and Ca^{2+}) from the dilute freshwater environment to replenish those lost by passive diffusion. The ionocytes are localised to the epithelial surfaces of the gill in adults and skin in larvae (Varsamos et al., 2005). In zebrafish (*Danio rerio*) larvae and, to a lesser extent, adults, ionocyte structure and function have been studied extensively (for reviews, see Hwang, 2009; Hwang and Perry, 2010; Hwang et al., 2011; Dymowska et al., 2012; Hwang and Chou, 2013; Guh et al., 2015), leading to the identification and characterisation of five ionocyte subtypes (Guh et al., 2015). H^+-ATPase-rich (HR) cells apically express a Na^+/H^+ exchanger paralog (NHE3b) and vacuolar-type H^+-ATPase (HA). Thus, the HR cells are involved in Na^+ uptake, acid extrusion and ammonia excretion (Lin et al., 2006; Esaki et al., 2007; Horng et al., 2007; Liao et al., 2007; Yan et al., 2007; reviewed by Kwong et al., 2014). A sub-population of Na^+/K^+-ATPase (NKA)-rich (NaR) cells contains epithelial Ca^{2+} channels (ECaC), basolateral plasma membrane Ca^{2+}-ATPase (PMCA) and basolateral Na^+/Ca^{2+} exchangers (NCX); the NaR cells are suggested to be involved in Ca^{2+} uptake (Liao et al., 2007). A second sub-population of NKA-enriched ionocytes that express the Cl^-/HCO_3^- exchanger SLC26 (Bayaa et al., 2009; Perry et al., 2009) have been termed SLC26 cells (Guh et al., 2015) and are thought to play a role in Cl^- uptake and HCO_3^- excretion. Na^+-Cl^--cotransporter rich (NCC) cells contain the titular transporter protein and are involved in absorption of both Na^+ and Cl^- (Wang et al., 2009). Finally, the K^+-secreting (KS) cells remain to be fully characterized, but were implicated in K^+ homeostasis owing to the presence of an orthologue of the renal outer medullary type K^+ (ROMK) channel localised uniquely in cells expressing the *a1a.4* isoform of NKA (Abbas et al., 2011).

Of the known five ionocyte subtypes in zebrafish larvae, the HR cell has been the most extensively studied owing to its multiple physiological roles, which include whole-body Na^+ regulation (Horng et al., 2007), systemic acid–base balance (presumed from measurements of cellular and whole-body acid secretion; Lin et al., 2006; Horng et al., 2007; Kumai et al., 2015) and excretion of nitrogenous waste, largely in the form of ammonia (Shih et al., 2008). Furthermore, the HR cell is conveniently visualized *in vivo* using the vital marker concanavalin A (ConA; Lin et al., 2006), which binds to surface glycoproteins containing α-D-mannose and α-D-glucose groups, and thus is readily amenable to *in vivo* measurements of H^+ secretion and NH_4^+ excretion using the scanning ion electrode technique (SIET; Lin et al., 2006; Horng et al., 2007; Shih et al., 2008). Indeed, the results of experiments employing SIET or radiotracer techniques when coupled with gene knockdown clearly demonstrate that the three physiological functions of the HR cell are intricately interrelated, thus establishing a strong linkage between Na^+ uptake, H^+ secretion and ammonia excretion in zebrafish larvae and presumably adults (Kumai and Perry, 2011, 2012; Shih et al., 2012). An additional feature of the HR cell model is the abundance of cytosolic carbonic anhydrase (CAc/CA2-like a; renamed to CA17a; Ferreira-Martins et al., 2016), which facilitates the intracellular production of H^+ (via

Department of Biology, University of Ottawa, 30 Marie Curie, Ottawa, ON KIN 6N5, Canada.

*Author for correspondence (sfperry@uottawa.ca)

S.F.P., 0000-0001-5819-2859

Received 22 August 2019; Accepted 28 January 2020

CO_2 hydration) to provide the necessary substrate for NHE3b and HA (Lin et al., 2008; reviewed by Gilmour and Perry, 2009). Although online genomic resources refer to CAc as '*ca2*', we feel that this nomenclature is inappropriate given the results of Esbaugh et al. (2005) showing that zebrafish CAc is distinct from tetrapod *ca2*. Thus, the zebrafish isoform will be hereafter referred to as CA17a.

Thus, in the larval zebrafish HR cell, there are thought to be two distinct pathways for acid secretion (via NHE3b or H^+-ATPase), both of which are dependent on the activity of CA. The presence of these acid secretion–Na^+ uptake pathways presumably enable the regulation of whole-body Na^+ and acid–base balance and may also facilitate intracellular pH (pHi) regulation within the HR cell itself. However, unlike for whole-body Na^+ uptake and acid secretion, the underlying mechanisms of pHi regulation in HR cells (or any other ionocyte subtype) have yet to be investigated. The lack of any data on ionocyte pHi regulation reflects, at least in part, the absence of a suitable technique for monitoring pHi in real time in cells of living fish. Therefore, an initial objective of the present study was to devise and validate a method to track pHi in HR cells *in vivo*. The next objective was to use this technique to investigate the potential role of three key proteins in HR cell acid–base regulation, namely NHE3b, HA and CA17a. We developed a method using the ratiometric pH-sensitive dye bis-carboxyethyl-carboxyfluorescein (BCECF) (Graber et al., 1986) in concert with the HR cell marker ConA to monitor pHi in HR cells on the yolk sac epithelium of larval zebrafish. Ultimately, pHi of HR cells was followed in real time when fish were challenged with exposure to conditions known to induce intracellular acidosis (using 1% CO_2) or alkalosis (using 20 mmol l^{-1} NH_4Cl; Boron and De Weer, 1976). By comparing the results obtained from control fish with those obtained from fish experiencing morpholino knockdown of CA17a, H^+-ATPase or NHE3b, and also clustered regularly interspaced palindromic repeats (CRISPR)/CRISPR-associated protein 9 (Cas9) knockout of *slc9a3.2* (encoding NHE3b), we were able to demonstrate important roles of these three proteins in HR cell intracellular acid–base balance, particularly during intracellular acidosis.

MATERIALS AND METHODS

Zebrafish

Adult wild-type zebrafish [*Danio rerio* (Hamilton 1822)] were supplied by Big Al's Aquarium Services (Ottawa, ON, Canada), and reared in aerated, recirculating, dechloraminated Ottawa tap water at 28°C (0.25 mmol l^{-1} Ca^{2+}, 0.78 mmol l^{-1} Na^+, 0.02 mmol l^{-1} K^+, 0.15 mmol l^{-1} Mg^{2+}, pH 7.6). An additional line of *slc9a3.2* knockout ('NHE3b mutant') fish was generated using CRISPR/Cas9 gene editing as described below. Fish were fed daily with No. 1 Crumble (Zeigler, Gardners, PA, USA) and subjected to a 14 h:10 h light:dark photoperiod. Embryos were obtained using standard breeding procedures (Westerfield, 1995) and reared in incubators at 28°C in 50 ml Petri dishes containing dechloraminated Ottawa tap water supplemented with 0.05% Methylene Blue. Water was changed daily and dead embryos were removed. All procedures were performed on 5 days post fertilization (dpf) zebrafish, in accordance with protocols approved by the University of Ottawa Animal Care Committee (BL-226, BL-1700) and in adherence to guidelines set by the Canadian Council of Animal Care (CCAC).

In vivo time-lapse ratiometric imaging

Zebrafish larvae at 5 dpf were anaesthetised in a bathing solution of dechloraminated Ottawa tap water containing 200 mg l^{-1} tricaine methanesulfonate (MS-222; Syndel Laboratories, Nanaimo, BC, Canada) and 1.05 mmol l^{-1} Tris base, adjusted to pH 7.6 with NaOH. Concanavalin A (ConA) was used to specifically label HR cells (Yan et al., 2007). Larvae were exposed to ConA (50 mg l^{-1})-Alexa Fluor 633 conjugate (Invitrogen, Waltham, MA, USA) and 50 µmol l^{-1} BCECF, acetoxymethyl ester (AM) dye (Invitrogen) for 25 min at room temperature. Larvae were washed in the initial bathing solution three times and immobilised inside a 35 mm Petri dish in 1.8% low-melting-point agarose (Bioshop, Burlington, ON, Canada) dissolved in the same solution. The agarose was heated in a microwave oven to just over the 63–67°C melting point, but was cooled down to a temperature slightly above the 26–28°C gelling point before being used to embed the larvae. After allowing the agarose to solidify for 20 min, the larvae were visualised using a Nikon Eclipse Ni-U upright microscope (Nikon Instruments, Tokyo, Japan) and images were captured using an Andor iXon Ultra EMCCD camera (Andor Technology, Belfast, UK). Larvae were maintained in the bathing solution provided with continuous water flow (see below) for an additional 30 min before the start of each experiment.

A gravity-driven continuous flow system was used to deliver various solutions (flow=1 ml min^{-1}) to larvae depending on experimental treatment; a vacuum pump was used to maintain a constant depth of fluid in the Petri dish. All solutions contained 200 mg l^{-1} MS-222 and 1.05 mmol l^{-1} Tris base to immobilise the larvae throughout the experiment. Solutions were maintained at room temperature and, if applicable, were aerated beginning from the start of the experiment. For each experiment, larvae were first exposed to a control solution (water with tricaine) for 10 min after which the specific experimental solution was delivered to the fish for 30 min. Subsequently, the larvae were re-exposed to the initial control solution for 30 min. Throughout the course of the experiment, the flow rate was maintained at approximately 1 ml min^{-1}, while the larvae were exposed at 20 s intervals to a sequence of LED excitation light pulses (438, 513 and 633 nm) using a Lumencor Spectra X light engine (Lumencor, Beaverton, OR, USA). Concurrently, emitted light was collected using a 535/20 nm filter for the first two wavelengths and a 700/75 nm filter for the 633 nm wavelength. Based on ConA staining and co-localisation with BCECF, three HR cells on the yolk sac of a single larva were designated as regions of interest (ROIs); an area spatially separated from the larva but still within the field of view was designated as background ROI. Emission intensity data from the ROIs were obtained from the 438 and 513 nm excitation channels and subtracted from the background intensity; the BCECF emission ratio was calculated by dividing the background-corrected 513 nm intensity by the background-corrected 438 nm intensity. Only experiments with surviving larvae (indicated by the presence of a heartbeat) at the end of the experiment were included in analyses.

Normalised ratio changes were obtained for three different experimental periods in the knockdown and knockout experiments. The 10–40 min period represents the change from baseline pHi that occurred in response to CO_2 or NH_4Cl. The 40–70 min period represents the change in pHi that occurred following the removal of the CO_2 or NH_4Cl. The 10–70 min period represents the change from baseline pHi that occurred after the exposure to CO_2/NH_4Cl and subsequent recovery following their removal.

Experimental treatments

The experimental solution used for the 10–40 min experimental treatment phase for each experiment varied as described below,

depending on the type of experiment to be performed: (1) control experiments, (2) respiratory acidosis and (3) metabolic alkalosis.

For proof of principle control experiments (1), the initial bathing solution was used in place of the experimental solution. Essentially, the same solution was used to perfuse the larvae throughout the entire 70-min experiment. To elicit respiratory acidosis (2), the initial bathing solution that had been equilibrated with 1% CO_2 for 30 min (pH 5.94) prior to the start of the experiment was used in the treatment phase of these experiments. To elicit metabolic alkalosis (3), 20 mmol l^{-1} NH_4Cl was added to the initial bathing solution, which was then pH-adjusted to 7.6 using NaOH and used in the treatment phase for these experiments.

Gene knockdown using antisense oligonucleotide morpholinos

For knockdown experiments, embryos were injected with antisense oligonucleotide morpholinos tagged with carboxyfluorescein (GeneTools, Philomath, OR, USA) at the one-cell stage. NHE3b (*slc9a3.2*; NM_001113479.1) was targeted using a morpholino that splices out exon two (5′-AGCTCAGTGACTGGAAAGAGAAAT-A-3′) (Kumai and Perry, 2011), while HA subunit A (*atpv1aa*; NM_201135.2) (5′-ATCCATCTTGTGTGTTAGAAAACTG-3′) and CA17a (*ca2*; NM_199215.2) (5′-TCGTATCCCCAGTGGTC-AGCCATTC-3′) were knocked down using morpholinos that targeted the ATG translational start codons (Horng et al., 2007; Lin et al., 2008; Lee et al., 2011). All morpholinos were prepared in 1× Danieau buffer [58 mmol l^{-1} NaCl, 0.7 mmol l^{-1} KCl, 0.4 mmol l^{-1} $MgSO_4$, 0.6 mmol l^{-1} $Ca(NO_3)_2$, 5 mmol l^{-1} Hepes; pH 7.6] containing 0.05% Phenol Red; 4 ng of morpholino was injected into each embryo, administered using an injection volume of 1 nl. Embryos were screened for the presence of carboxyfluorescein at 1 dpf and only carboxyfluorescein-positive embryos were used for subsequent experiments. Successful knockdown was verified by reverse transcriptase PCR (RT-PCR), western blotting or immunohistochemistry.

Gene knockout using CRISPR/Cas9 gene editing

slc9a3.2 (encoding NHE3b) was knocked out using CRISPR/Cas9. A single-guide RNA (sgRNA) was synthesized using a method described previously (Talbot and Amacher, 2014) and the guide sequence of the sgRNA, specific to a region of exon 1 of *slc9a3.2* (TGCATTACATGAGGCTGCTG), was selected using online software (CHOPCHOP; Montague et al., 2014; Labun et al., 2016). sgRNA size and quality were verified by gel electrophoresis, and RNA concentration was determined spectrophotometrically following purification (RNeasy Mini Kit, QIAGEN, Hilden, Germany). Cas9 mRNA was synthesised from zebrafish codon-optimised Cas9 (pCS2-nls-zCas9-nls; Jao et al., 2013) using a commercial kit (mMESSAGE mMACHINE SP6 kit, Invitrogen). Following purification (RNeasy Mini Kit, QIAGEN), mRNA size and quality was checked by gel electrophoresis and concentration was determined spectrophotometrically.

Wild-type one-cell embryos were injected with 1 nl of injection solution containing 150 pg Cas9 mRNA, 50 pg of sgRNA, and 0.05% Phenol Red suspended in Danieau buffer. Injected fish were reared to sexual maturity (60–90 dpf), and mutants in this adult F0 population were identified through DNA extraction (tissue digestion in 50 mmol l^{-1} NaOH for 10 min at 95°C) of fin clips and Sanger sequencing (Genome Quebec, McGill University, Montreal, Canada) which confirmed that a portion (~80%) of the embryos had a mutated *slc9a3.2* gene. A mutant line (termed 'NHE3b mutants') was then established using a standard breeding protocol (Zimmer et al., 2019a,b; Zimmer et al., 2020) from founders carrying a 5-bp deletion mutation that resulted in a predicted premature stop codon. Effective knockout of *slc9a3.2* was confirmed by immunohistochemistry using adult gill filaments (see below); experiments were performed on the F3 generation of this founding population.

Reverse transcriptase polymerase chain reaction (RT-PCR)

Knockdown of NHE3b with a splice-blocking morpholino was verified using RT-PCR (Kumai and Perry, 2011). Whole-body mRNA was extracted from pools of 30 larvae at 4 dpf using Trizol (Invitrogen) according to manufacturer's specifications. cDNA was synthesised by treating 1 µg of extracted RNA with DNase (Invitrogen) and RevertAid M-MNuLV reverse transcriptase (Fermentas, Burlington, ON, Canada), as per the manufacturer's protocol. PCR primers for NHE3b were forward 5′-TCCTGAAAC-ACCACGATTCA-3′ and reverse 5′-ACAGGGTCCACAGCAGA-CAT-3′ (Kumai and Perry, 2011). PCR conditions were as follows: initial denaturation at 94°C for 1 min, followed by 30 cycles of 94°C for 30 s, 58°C for 30 s and 72°C for 1 min, and a final extension at 72°C for 5 min. Primers for 18S rRNA were used to confirm equal loading (forward primer 5′-GGCGGCGTTATTCCCATGACC-3′; reverse primer 5′-GGTGGTGCCCTTCCGTCAATTC-3′). All PCR products were run on a 1% agarose gel and imaged with a Gel doc system equipped with the Quantity-One 1-D analyzer software (Bio-Rad, Mississauga, ON, Canada).

Western blotting

To verify knockdown of CA17a, protein was extracted from pools of 20 larvae using RIPA buffer (150 mmol l^{-1} NaCl, 1% Triton X-100, 0.5% sodium deoxycholate, 0.1% SDS, 50 mmol l^{-1} Tris-Cl, 1 mmol l^{-1} EDTA, 1 mmol l^{-1} phenylmethanesulfonyl fluoride) containing a cocktail of protease inhibitors (Roche, Mississauga, ON, Canada). Larval homogenates were then run on 10% SDS-PAGE gel at 200 V and transferred onto a polyvinylidene fluoride (PVDF) membrane (Bio-Rad), using a Trans-Blot SD Semi-Dry Transfer Cell (Bio-Rad) running at 25 V for 1 h. The membranes were blocked with 5% skim milk in 0.05% Tween-20 in Tris buffer saline (TBS-T) for 2 h at room temperature, followed by incubation with custom-made rabbit polyclonal primary antibodies specific to CA17a (antigen sequence WGYDKHNGPDKWGC, 1:1000 dilution of an initial stock concentration 2.01 mg ml^{-1}, Genscript, Piscataway, NJ, USA; Miller et al., 2014) in 2% skim milk in 0.05% TBS-T, at 4°C overnight. After washing with 0.05% TBS-T 3× for 5 min each, the membranes were incubated with a horseradish peroxidase (HRP)-conjugated goat anti-rabbit secondary antibody (1:5000 dilution; product no. 65-6120, Invitrogen) in 2% skim milk in 0.05% TBS-T for 1 h at room temperature. Membranes were then washed 5× for 5 min each and bands were visualised using enhanced chemiluminescence (SuperSignal West Femto chemiluminescent substrate, Pierce Biotechnology, Waltham, MA, USA) on a XRS+ ChemiDoc system (Bio-Rad). The membrane was then re-probed using a monoclonal β-actin antibody raised in mouse (Product No. A3854; 1:4000 dilution; Sigma-Aldrich, St Louis, MO, USA) after being stripped with ReBlot Plus antibody stripping solution (Millipore, Billerica, MA, USA) according to the manufacturer's specifications.

Whole-mount immunohistochemistry

To verify the knockdown of HA, live larvae were first exposed to the ConA-Alexa Fluor 633 conjugate (50 µg ml^{-1}; Invitrogen) for 25 min at room temperature and then were euthanised with an

overdose of MS-222 at pH 7.6. The samples were then fixed at 4°C overnight using 4% paraformaldehyde (PFA) in PBS, followed by a stepwise dehydration in 100% MeOH in three 5-min washing steps. Samples were kept in 100% MeOH at −20°C until further analysis. To verify knockout of NHE3b, gill baskets were excised from wild-type and NHE3b mutant adult zebrafish and were fixed in 4% PFA in PBS overnight at 4°C. Following fixation, individual filaments were isolated from the gill arches to ensure consistent and even antibody probing. Prior to immunostaining, dehydrated larvae were rehydrated in three stepwise 5-min washing steps in PBS containing 0.1% Tween 20 (PBS-T). Thereafter, both larval and gill filament samples were treated in a similar manner. Antigen retrieval was performed on gill filament samples by incubating samples in 150 mmol l^{-1} Tris-HCl (pH 9) for 10 min at room temperature followed by 15 min at 65°C. Following five rinses in PBS-T, samples were then permeabilised by incubation at room temperature with a solution of 3% BSA containing 0.8% Triton X-100 in PBS-T for 1 h. Immediately afterwards, the samples were incubated overnight at 4°C with primary antibodies. Larvae were probed with a rabbit polyclonal antibody specific to a region of the A subunit of bovine HA (antigen sequence AEMPADSGYPAYLGAR, 1:4000 dilution of unknown initial stock concentration; antibody obtained from Professor Minoru Uchiyama, formerly affiliated with the University of Toyama, Japan, 100% sequence identity with zebrafish; Ura et al., 1996). Gill filaments were probed with a custom-made rabbit polyclonal antibody specific to NHE3b (antigen sequence CEPAADEETPEEKPA, 1:200 dilution of an initial 1.10 mg ml^{-1} stock concentration, Genscript) and a mouse monoclonal antibody specific to the α subunit of Na^+/K^+-ATPase (α5; 1:250 dilution; Developmental Studies Hybridoma Bank, University of Iowa, Ames, IA, USA) (Takeyasu et al., 1988) in 3% BSA, 0.8% Trion X-100 in 0.1% PBS-T. Samples were then rinsed with 0.1% PBS-T 3× and, for larvae, were incubated in donkey anti-rabbit secondary antibody conjugated with Alexa Fluor 568 (1:500 dilution, Invitrogen) or, for gill filaments, were incubated in donkey anti-rabbit secondary antibody conjugated with Alexa Fluor 568 (1:500 dilution, Invitrogen) and goat anti-mouse secondary antibody conjugated with Alexa Fluor 488 (1:500 dilution, Invitrogen) in 3% BSA, 0.8% Triton X-100 in PBS-T. After five washes of 5 min each with 0.1% PBS-T, larvae were mounted on concave glass slides (Fisher Scientific, Waltham, MA, USA), while gill filaments were separated out and mounted on concave glass slides as well. Images were then captured using an A1R+ confocal microscope (Nikon Instruments). Solid state lasers emitting at 488, 561 and 633 nm were used for excitation of fluorophores, and images were composed using maximum intensity projection of Z-stacks of 30 µm thickness composed of 30 optical sections of 1 µm each. Immunohistochemistry was used as the method of choice for verification because the aforementioned antibodies did not yield reliable data when used in western blots. All samples within the same experiment were imaged using the exact same optical configurations, and no post-acquisition processing was applied to the images.

Statistical analysis

For each experiment, data were obtained from three cells from a single larva and averaged to yield N=1. For graphing and statistical purposes, a reference ratio value was determined for each cell; using the average of 10 data points (representing a total of 20×10=200 s) before (and including) the point at the 10-min mark of each experiment, each ROI was normalised to a value of 1. Relative normalised ratio data were calculated for all time points prior to and following this reference period by dividing the reference ratio.

To calculate the maximum normalised ratio change during and after each 30-min experimental treatment (see below), each 20-s ratio measurement interval was averaged with the next nine ratio measurements to obtain a series of 10-point average ratio values, spanning a total interval of 3 min for each measurement. For acidosis experiments, the minimum 10-point average ratio value during the 10–40 min period of exposure to CO_2 and the maximum 10-point average ratio value for the 40–70 min post-CO_2 periods were selected. Conversely, for alkalosis experiments, the maximum 10-point average ratio value during the 10–40 min period of exposure to NH_4Cl and the minimum 10-point average ratio value for the 40–70 min post-NH_4Cl periods were selected. A single set of control data was used in the proof of principle experiments and the appropriate method was applied depending on whether the data were being compared with CO_2- or NH_4Cl-treated fish. The significance of the difference between these points was assessed within each experiment using one-way repeated-measures ANOVA and the Holm–Šidák test for comparisons between sets. Additionally, for morphant/knockout versus sham/wild-type experiments, the maximum differences between the points were compared between morphant/knockout and sham/wild-type experiment sets (10–40, 40–70 and 10–70 min), using Student's t-tests. All P-values <0.05 were reported as statistically significant. A similar statistical approach was used to determine significant differences between shams/wild-types and morphants/knockouts in the time required to reach minimum/maximum relative ratio values during the 10–40 min treatment period and the 40–70 min post-treatment periods.

RESULTS

Proof of principle experiments

To specifically monitor relative pHi changes in HR cells, ROIs (cells) were selected based on co-localisation of ConA and BCECF staining (Fig. 1A). A series of experiments was conducted to demonstrate that the BCECF 513/438 ratio was a reliable indicator of relative changes in pHi of HR cells during acute experimental manipulations. The control fish bathed continually with flowing aerated bathing solution did not display a significant change in BCECF 513/438 ratio values during 70 min of recording (Fig. 1B). Exposure of fish to hypercapnia (1% CO_2), a treatment expected to induce intracellular acidosis, caused a significant decrease in the BCECF 513/438 ratio that appeared to be reduced maximally after 30 min of treatment (Fig. 1C). Restoration of normocapnia caused the BCECF 513/438 ratio to return to baseline values within 30 min (Fig. 1B). Exposure to 20 mmol l^{-1} NH_4Cl, a treatment known to induce intracellular alkalisation, was accompanied by a significant increase in the BCECF 513/438 ratio which was followed by a significant decrease below baseline levels 30 min after the NH_4Cl was washed out (Fig. 1D). Thus, for the remainder of this paper it is assumed that decreases and increases in the BCECF ratios represent decreases and increases in pHi, respectively.

Effects of CA17a knockdown on CO_2-induced acidosis and NH_4^+-induced alkalosis

An antisense morpholino was used to investigate the role of CA17a in regulating HR cell pHi in the face of acute acidosis or alkalosis. To confirm that the expression of CA17a was indeed suppressed in the morphants, qualitative western blot analysis was performed. In morphants, there was a clear elimination of the band at ∼30 kDa (based on three separate western blots) corresponding to the expected molecular weight of CA17a; the intensity of the β-actin bands was similar in shams and morphants (Fig. 2A). Similar

Journal of Experimental Biology (2020) 223, jeb212928. doi:10.1242/jeb.212928

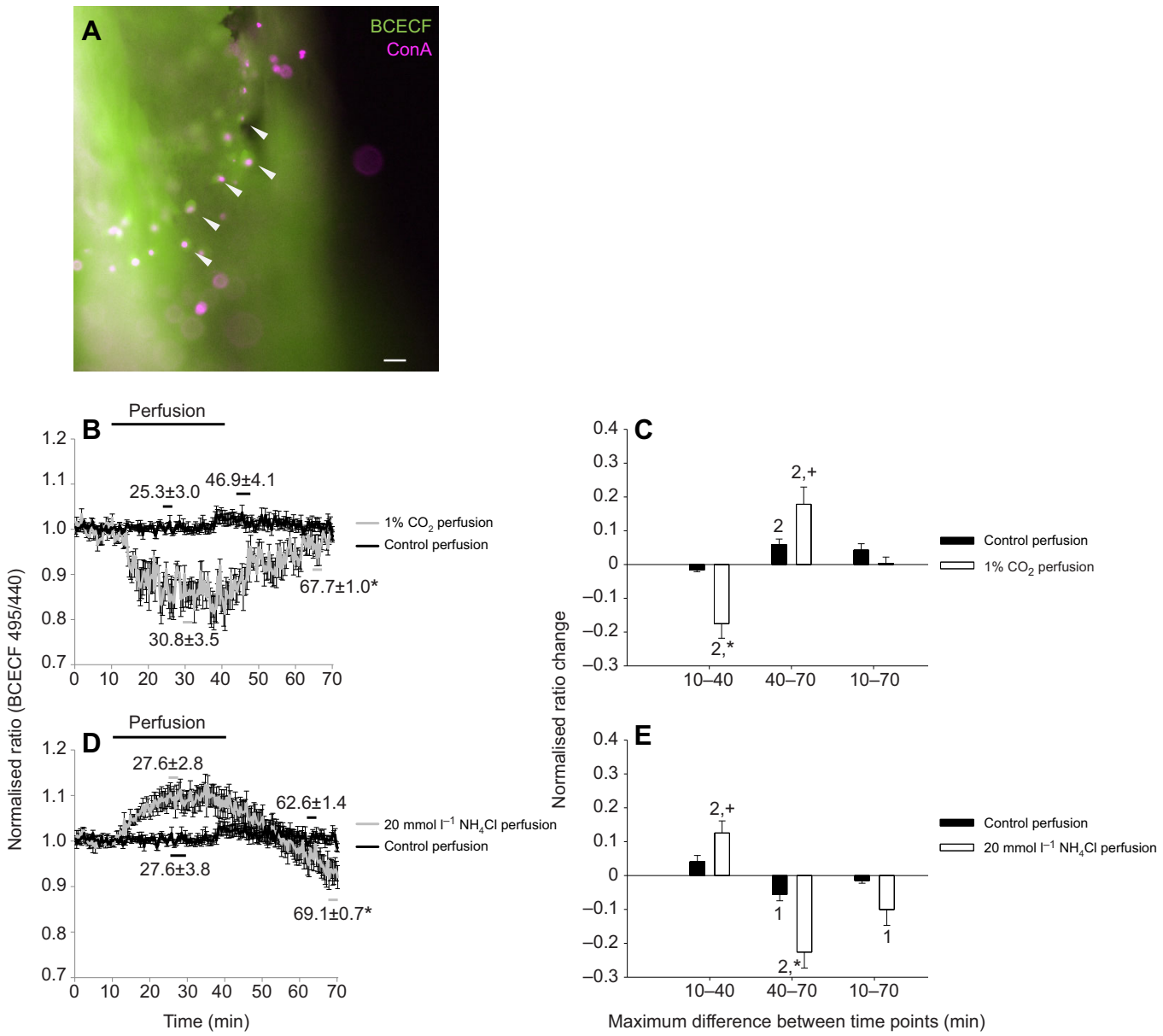

Fig. 1. *In vivo* ratiometric imaging of H$^+$-ATPase-rich (HR) cells on the yolk sac epithelium of zebrafish larvae at 5 days post fertilization (dpf) using the pH indicator BCECF. (A) Cells targeted for imaging were selected based on co-localization of BCECF and the HR cell marker Concanavalin A (ConA; white arrowheads). Scale bar: 20 µm. Larvae were bathed initially for 10 min with flowing aerated water containing anaesthetic followed by continued delivery for 30 min of either aerated water (*N*=4) or water equilibrated with 1% CO_2 (*N*=4) or containing 20 mmol l^{-1} NH_4Cl (*N*=8). Comparisons are made between control versus 1% CO_2 perfusion (B) and control versus 20 mmol l^{-1} NH_4Cl perfusion (D). Horizontal lines above the graphs indicate the durations of CO_2, NH_4Cl or control water exposures. The reference points in B and D indicate the averaged maximum/minimum emission ratios during the treatment period (10–40 min) and the averaged maximum/minimum ratios during the post-treatment period (40–70 min). Values indicated on each point refer to the means±s.e.m. of each of the corresponding time points chosen [maximum or minimum normalized BCECF ratios during the 30 min treatment period (10–40 min) or the 30 min recovery period (40–70 min)]. Bar graphs illustrate the changes in normalised BCECF 513/438 ratios between the indicated reference points within the specified time periods (C,E). Significant differences (*P*<0.05; Student's *t*-test) between CO_2/NH_4Cl and control treatments are indicated by asterisks (two-tailed test) or crosses (one-tailed test). The number 2 on the bar graphs represents *P*<0.05 (two-tailed one-sample *t*-test) while the number 1 represents *P*<0.05 (one-tailed one-sample *t*-test) that the ratio change is significantly different from 0.

efficacy of CA knockdown using the same morpholino was demonstrated previously (Miller et al., 2014).

The fish exposed to 1% CO_2 exhibited significant acidosis and a subsequent increase in pHi in the sham and morphant fish when 1% CO_2 was removed (Fig. 2B). However, there were obvious temporal and response magnitude differences between the morphant and sham fish. For example, the sham fish attained a maximal reduction in pHi at 27.5±1.0 min, after which it remained stable, compared with 38.7±0.7 min in the morphants (Fig. 2B). Although the magnitude of intracellular acidification during the period of CO_2 exposure was not statistically different between the sham and morphant fish (Fig. 2C; *P*=0.11), the magnitude of pHi recovery upon removal of CO_2 was significantly reduced in the morphants (Fig. 2C). The CA17a morphant fish appeared to exhibit a similar initial rate of return to baseline pHi as the sham fish (Fig. 2B), but by the end of the recovery period (70 min), pHi was significantly reduced compared with shams

Journal of Experimental Biology (2020) 223, jeb212928. doi:10.1242/jeb.212928

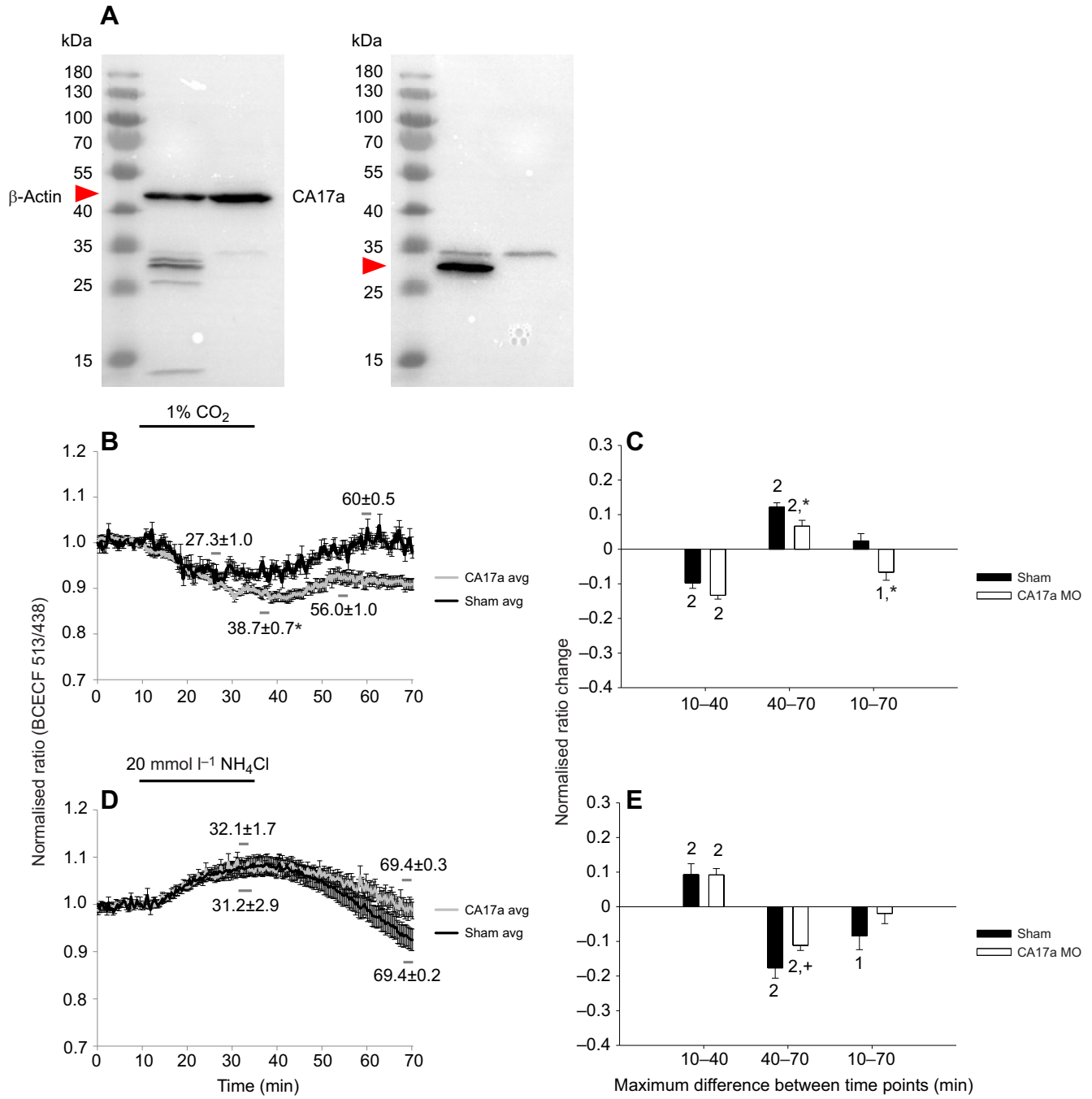

Fig. 2. The effects of CA17a knockdown on relative intracellular pH (pHi) changes (monitored using *in vivo* BCECF ratiometric imaging) in HR cells of zebrafish larvae at 5 dpf subjected to respiratory acidosis or metabolic alkalosis. The representative western blot (A) illustrates the absence of CA17a protein (red arrowhead) in the morphant fish. After 10 min of baseline recording, fish were exposed for 30 min to either 1% CO_2 (B,C; *N*=4) or 20 mmol l^{-1} NH_4Cl (D,E; *N*=6). Bars above graphs (B,D) indicate the 30 min periods of exposure to CO_2 or NH_4Cl. Changes in the BCECF 513/438 emission ratio correlate positively to changes in pHi. The reference points in B and D indicate the averaged maximum/minimum emission ratios during the treatment period (10–40 min) and the averaged maximum/minimum ratios during the post-treatment period (40–70 min). Values indicated on each point refer to the means±s.e.m. of each of the corresponding time points chosen [maximum or minimum normalized BCECF ratios during the 30 min treatment period (10–40 min) or the 30 min recovery period (40–70 min)]. Bar graphs illustrate the changes in normalised BCECF 513/438 ratios between the indicated reference points within the specified time periods (C,E). Significant differences (P<0.05; Student's *t*-test) between shams and morphants (MO) are indicated by asterisks (two-tailed test) or crosses (one-tailed test). The number 2 on the bar graphs represents P<0.05 (two-tailed one-sample *t*-test) while the number 1 represents P<0.05 (one-tailed one-sample *t*-test) that the ratio change is significantly different from 0.

(Fig. 2C). These data indicate a significantly reduced capacity of CA17a morphants to regulate pHi after acute hypercapnia.

The time course and extent of intracellular alkalisation were similar in shams and CA17a morphants exposed to 20 mmol l^{-1} NH_4Cl (Fig. 2D,E). However, unlike in the sham fish, the HR cells of the CA17a morphants did not undershoot baseline pHi within 30 min after the washout of NH_4Cl (Fig. 2E). Indeed, the extent of intracellular acidosis during the 30 min after NH_4Cl washout was

Journal of Experimental Biology (2020) 223, jeb212928. doi:10.1242/jeb.212928

significantly reduced (one-tailed *t*-test). The time required for sham and morphant fish to reach the maximum point during NH_4Cl treatment and the minimum point after NH_4Cl washout were not significantly different (Fig. 2D).

Effects of NHE3b knockdown or knockout on CO_2-induced acidosis and NH_4^+-induced alkalosis

RT-PCR was used to demonstrate the success of NHE3b knockdown; there was a clear reduction in the intensity of the band of interest at 700 bp, while the band intensities for 18S mRNA in NHE3b morphants and sham controls were similar (Fig. 3A).

Similar to the CA17a morphants, pHi in the NHE3b morphants declined through most of the period of CO_2 exposure until 37.9± 0.6 min, which was significantly longer than in the shams at 29.2± 1.2 min (Fig. 3B). pHi also decreased to a greater extent in NHE3b morphants compared with shams after 30 min (Fig. 3C). Additionally, upon return to normocapnia, the extent of the alkalisation was significantly blunted in the NHE3b morphants (Fig. 3B,C). Over the course of the entire 60 min experiment, the NHE3b morphants underwent a net decrease in pHi whereas the shams underwent a net increase (Fig. 3B). Thus, after 70 min, pHi in the morphants and shams had diverged such that the net

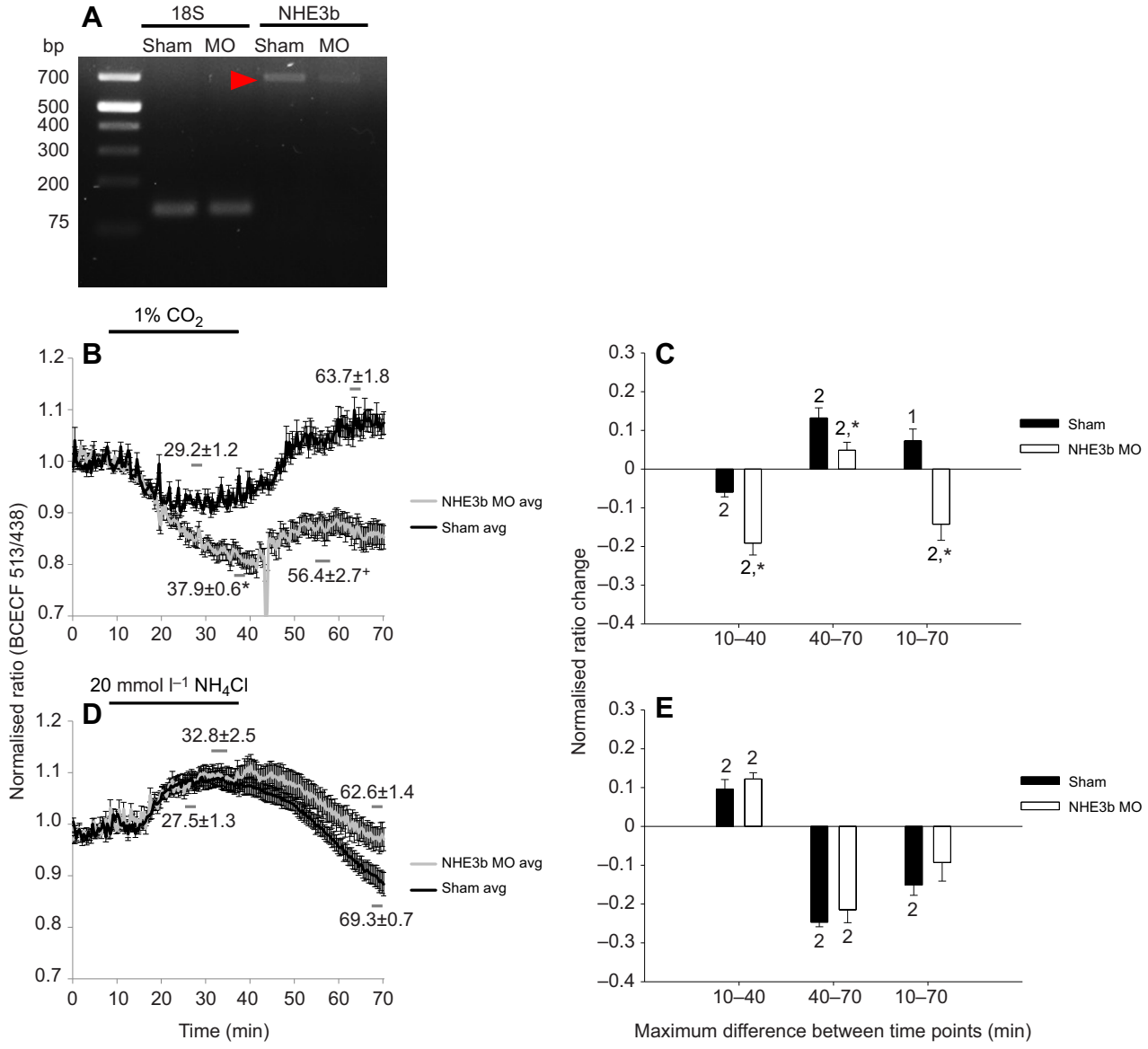

Fig. 3. The effects of NHE3b knockdown on relative pHi changes (monitored using *in vivo* BCECF ratiometric imaging) in HR cells of zebrafish larvae at 5 dpf subjected to respiratory acidosis or metabolic alkalosis. The representative RT-PCR gel (A) illustrates the absence of the 700 kDa PCR product (red arrowhead) in the morphant fish. After 10 min of baseline recording, fish were exposed for 30 min to either 1% CO_2 (B,C; *N*=4) or 20 mmol l^{-1} NH_4Cl (D,E; *N*=4). Bars above graphs (B,D) indicate the 30 min periods of exposure to CO_2 or NH_4Cl. The reference points in B and D indicate the averaged maximum/minimum emission ratios during the treatment period (10–40 min) and the averaged maximum/minimum ratios during the post-treatment period (40–70 min). Numbers indicated on each point refer to the means±s.e.m. of each of the corresponding time points chosen [maximum or minimum normalized BCECF ratios during the 30 min treatment period (10–40 min) or the 30 min recovery period (40–70 min)]. Bar graphs illustrate the changes in normalised BCECF 513/438 ratios between the indicated reference points within the specified time periods (C,E). Significant differences (P<0.05; Student's *t*-test) between shams and morphants (MO) are indicated by asterisks (two-tailed test) or crosses (one-tailed test). The number 2 on the bar graphs represents P<0.05 (two-tailed one-sample *t*-test) while the number 1 represents P<0.05 (one-tailed one-sample *t*-test) that the ratio change is significantly different from 0.

Journal of Experimental Biology (2020) 223, jeb212928. doi:10.1242/jeb.212928

changes in normalised ratios over 60 min were significantly different (Fig. 3C).

The extent of intracellular alkalisation during NH_4Cl exposure and relative intracellular acidification during the NH_4Cl washout phase were similar in the sham and NHE3b morphant fish (Fig. 3D,E). NHE3b morphants behaved similarly to the shams with respect to the time required to reach the maximum point during NH_4Cl treatment and the minimum point post-treatment (Fig. 3D).

Knockout of *slc9a3.2* was demonstrated at the genomic level by Sanger sequencing (Fig. S1) and immunohistochemistry of gill filaments extracted from adult wild-type (Fig. 4A) and mutant (Fig. 4B) fish. Loss of NHE3b was demonstrated by the lack of Alexa Fluor 568 staining in the mutants (Fig. 4B).

There was no significant difference in the degree of acidification during 1% CO_2 exposure in the wild-type and NHE3b knockouts (Fig. 4D). However, the HR cells in the NHE3b knockout fish continued to experience a decline in pHi well after the cells of the wild-type fish had plateaued (37.1±1.2 min versus 30.7±3.2 min, respectively; Fig. 4C), a trend that was also observed in the NHE3b morphants (Fig. 3B). Also similar to the results of the NHE3b morphant experiment, albeit less pronounced, the post-hypercapnic increase in pHi was significantly greater in the wild-type fish compared with the NHE3b knockouts (Fig. 4D). Indeed, at 70 min, HR cells of wild-type fish did not display a significant difference from the original baseline pHi, while HR cells in knockout fish showed a significantly lower pHi compared with the original baseline (10–70 min; Fig. 4D).

Effects of HA knockdown on CO_2-induced acidosis and NH_4^+-induced alkalosis

Immunohistochemistry was used to demonstrate the successful knockdown of HA in the morphants. Although western blotting would be the preferred method for validation, we experienced no success using the HA antibodies for western blotting (A.M.Z.,

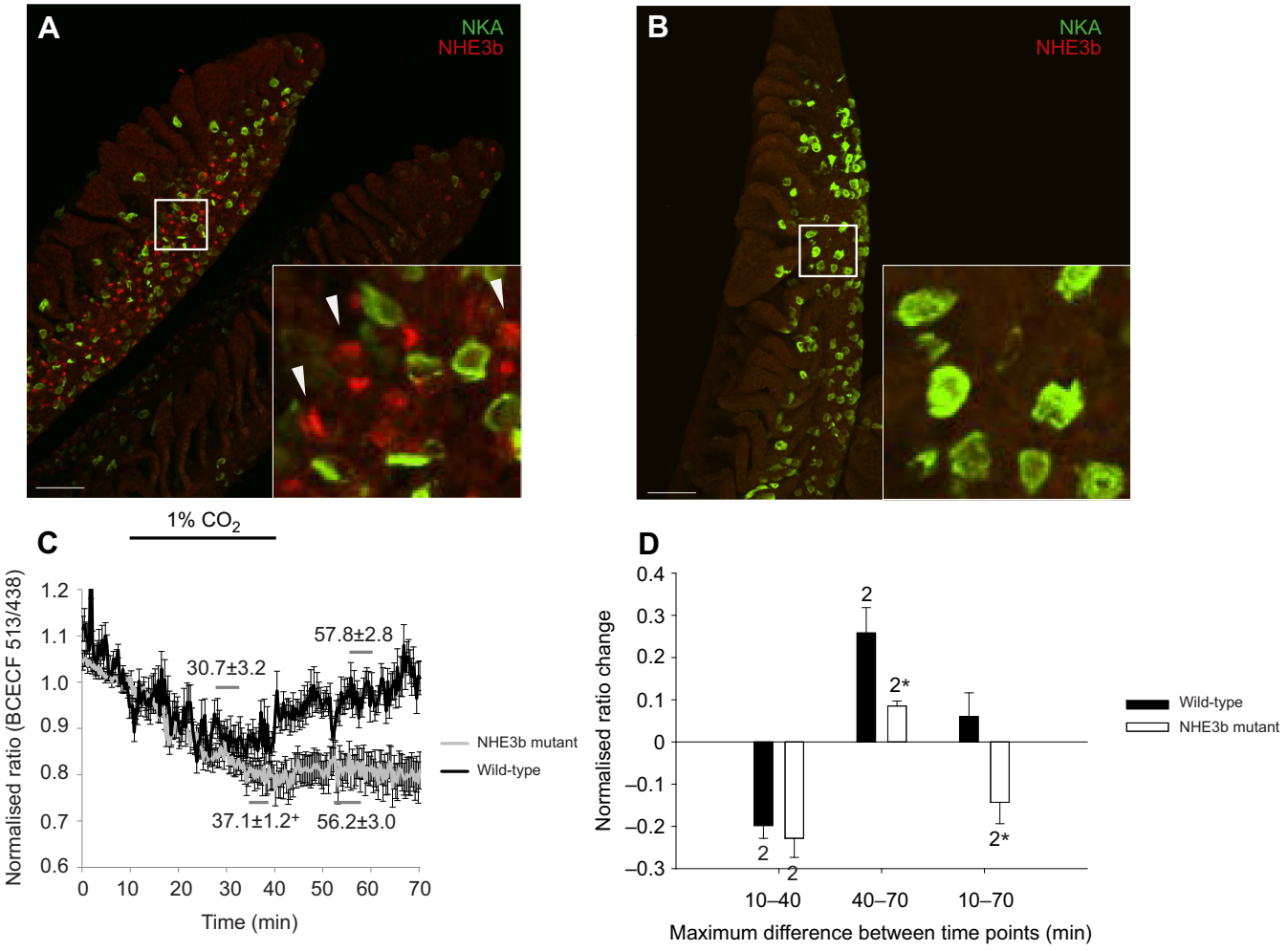

Fig. 4. The effects of NHE3b gene knockout on relative pHi changes (monitored using *in vivo* BCECF ratiometric imaging) in HR cells of zebrafish larvae at 5 dpf subjected to respiratory acidosis or metabolic alkalosis. Representative whole-mount immunohistochemistry images indicate the presence (A) or absence (B) of NHE3b staining (red) in wild-type and mutant adult gill filaments. White arrows indicate cells expressing NHE3b. Scale bar: 50 μm. After 10 min of baseline recording, fish were exposed for 30 min to 1% CO_2 (B; N=6). The bar above the data in C indicates the 30 min period of exposure to CO_2. The reference points in C indicate the averaged maximum/minimum emission ratios during the treatment period (10–40 min) and the averaged maximum/minimum ratios during the post-treatment period (40–70 min). Values indicated on each point refer to the means±s.e.m. of each of the corresponding time points chosen [maximum or minimum normalized BCECF ratios during the 30 min treatment period (10–40 min) or the 30 min recovery period (40–70 min)]. Bar graph illustrates the changes in normalised BCECF 513/438 ratios between the indicated reference points within the specified time periods (D). Significant differences (P<0.05; Student's t-test) between shams and knockouts are indicated by asterisks (two-tailed test) or crosses (one-tailed test). The number 2 on the bar graph represents P<0.05 (two-tailed one-sample t-test) while the number 1 represents P<0.05 (one-tailed one-sample t-test) that the ratio change is significantly different from 0.

Journal of Experimental Biology (2020) 223, jeb212928. doi:10.1242/jeb.212928

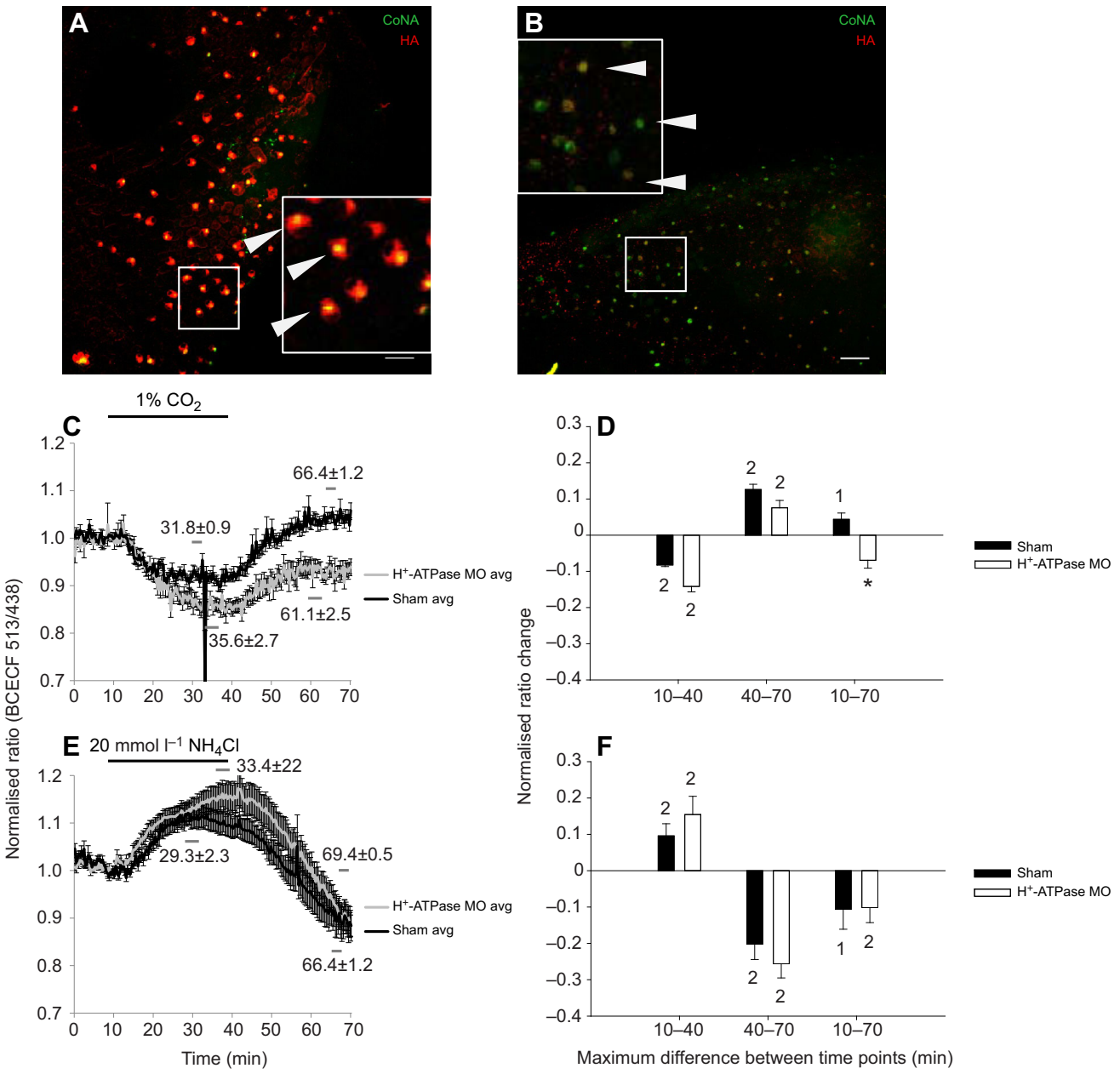

Fig. 5. The effects of H$^+$-ATPase (HA) knockdown on relative pHi changes (monitored using *in vivo* BCECF ratiometric imaging) in HR cells of zebrafish larvae at 5 dpf subjected to respiratory acidosis or metabolic alkalosis. Representative whole-mount immunohistochemistry images indicate the presence (A) or absence (B) of co-localisation between ConA (green) and HA (red) staining in sham and HA morphants. White arrows indicate HR cells. Scale bar: 20 μm. After 10 min of baseline recording, fish were exposed for 30 min to either 1% CO_2 (B,C; *N*=4) or 20 mmol l^{-1} NH_4Cl (D,E; *N*=6). Bars above graphs (B,D) indicate the 30 min periods of exposure to CO_2 or NH_4Cl. The reference points in B and D indicate the averaged maximum/minimum emission ratios during the treatment period (10–40 min) and the averaged maximum/minimum ratios during the post-treatment period (40–70 min). Numbers indicated on each point refer to the means±s.e.m. of each of the corresponding time points chosen [maximum or minimum normalized BCECF ratios during the 30 min treatment period (10–40 min) or the 30 min recovery period (40–70 min)]. Significant differences (P<0.05; Student's *t*-test) between shams and morphants (MO) are indicated by asterisks (two-tailed test) or crosses (one-tailed test). The number 2 on the bar graphs represents P<0.05 (two-tailed one-sample *t*-test) while the number 1 represents P<0.05 (one-tailed one-sample *t*-test) that the ratio change is significantly different from 0.

unpublished data). The representative images depicted in Fig. 5 clearly illustrate abundant expression of HA in the ConA-positive HR cells (Fig. 5A) of shams that was absent in the ConA-positive HR cells of the morphants (Fig. 5B).

The exposure of fish to 1% CO_2 and their subsequent return to normocapnic conditions revealed two significant differences between the HA and the previous two morphants. First, pHi of HR cells in the morphants stabilised at the 35.6±2.7 min time point, which was not significantly different from the sham fish at 31.8±0.9 min (Fig. 5C), and the maximal absolute intracellular acidification achieved within 30 min of CO_2 exposure did not differ significantly between the morphants and the shams (Fig. 5D). This contrasted with the significant differences in time points observed during CO_2-induced acidosis in the CA17a (Fig. 3) morphants, and in both time points and magnitude in NHE3b (Fig. 2) morphants. Second, although the morphants and the sham larvae exhibited similar rates of pHi recovery during the post-CO_2 treatment period, there was a significant difference in the extent of

Journal of Experimental Biology (2020) 223, jeb212928. doi:10.1242/jeb.212928

the pHi change between the shams and morphants at the conclusion of the experiments relative to the initial pHi baseline (Fig. 5D). This contrasted with the significantly blunted post-CO_2 recovery observed in both NHE3b (Fig. 2) and CA17a (Fig. 3) morphants.

For the NH_4Cl experiments, the HR cells from both HA morphants and shams exhibited a significant increase in pHi during the 30 min exposure phase and a significant decrease in pHi during the period following its washout (Fig. 5E). There were no differences in the time courses or extent of pHi changes between the shams and morphants (Fig. 5E,F).

DISCUSSION

To our knowledge, only one previous study successfully monitored relative pHi changes *in vivo* and in real time. The previous study (Molich and Heisler, 2005) was conducted by direct injection of the SNARF-1 ratiometric dye into zebrafish embryos at a very early developmental stage, and fish were monitored only until the end of epiboly (~10 h post fertilisation). For the present study, a subtype of zebrafish ionocyte, the HR cell, was targeted because of the wealth of existing data surrounding its H^+ secretory pathways and its straightforward identification *in vivo* using the vital fluorescently tagged HR cell marker, ConA. The principal novel finding of the present study is that three components of the Na^+ uptake/H^+ extrusion pathways contribute to pHi regulation in HR cells in response to respiratory acidosis: namely, the catalysed production of H^+ from CO_2 via CA17a, Na^+/H^+ exchange via NHE3b and active H^+ secretion via V-type H^+-ATPase. Yet, none of these pathways appear to contribute significantly to regulation of HR intracellular alkalosis induced by NH_4Cl aside from a small contribution from CA17a.

A critique of the methods

The BCECF 513/438 ratios are presented in a form normalised to the baseline ratio values of each individual experiment, instead of presenting the raw BCECF 513/438 ratio values. As mentioned earlier, BCECF 513/438 ratio values vary substantially between individual experiments. Thus, although the microscope settings and experimental parameters remained constant between experiments, slight differences in other factors such as yolk auto fluorescence, relative positioning of HR cells and gel thickness can cause variations in the acquired BCECF 513/438 ratios, even when recording from multiple cells from the same larva. Because HR cells are expected to exhibit a consistent and narrow pHi range when exposed to similar conditions, the normalised ratio values are more useful in capturing the relative changes of pHi in the cells exposed to acid–base challenges. Perhaps the greatest limitation of this normalisation procedure is the inability to assess whether absolute pHi in HR cells changed with the gene knockdown/knockout treatments. Ultimately, this limitation prevents us from calculating ΔpHi and thus to be valid, any comparisons of rates of intracellular acidification or alkalisation with treatment would require that initial pHi values be similar among the treatments. Regardless, in the absence of a suitable calibration technique (see below), the data must be presented in a normalised manner.

Currently, a major limitation with the *in vivo* ratiometric pHi imaging technique is the inability to measure absolute *in vivo* pHi values. Our attempts to calibrate pHi using the K^+/nigericin (Montrose and Murer, 1986) and carbonyl cyanide m-chlorophenyl hydrazone (CCCP; James-Kracke, 1992) calibration methods, both of which have been known to work on cell cultures (Boyarsky et al., 1996), all resulted in the death of the larvae when exposed to the necessary concentrations. Also, the widely varying absolute 513/438 emission ratio values between individual experiments render *in vitro* calibrations unfeasible. To allow the measurement of absolute pHi values in cells of interest in a consistent and reproducible manner in future experiments, the creation of a method to calibrate the pHi of cells of viable zebrafish larvae is of utmost importance.

For unknown reasons, the homologous NHE3b antibody, although effective in staining NHE3b in adult gill (Fig. 4), failed to detect NHE3b expression in wild-type larvae despite being tested using a variety of immunohistochemistry protocols. Its low expression in larvae relative to the adult gill (Ito et al., 2013) may in part explain the inability to detect NHE3 with immunohistochemistry using the homologous antibody. However, clear evidence of NHE3b expression in larvae HR cells was provided using an antibody designed against the rainbow trout orthologue (Zimmer et al., 2019a,b), with one of the two peptide antigens sharing 91% amino acid identity (19/21 identical amino acids) with the corresponding sequence of zebrafish NHE3b. Fig. S2 demonstrates localisation of NHE3b in a sub-population of ConA-positive HR cells, confirming the previous result of Ito et al. (2013).

Proof of principle experiments

Given that the BCECF emission ratios could not be converted to absolute pHi data, it was critical to demonstrate that HR cells experiencing respiratory acidosis (by exposure to 1% CO_2) or metabolic alkalosis (by exposure to 20 mmol l^{-1} NH_4Cl) exhibited BCECF 513/438 emission ratios indicative of the pHi changes expected to accompany such treatments. Thus, it was predicted that exposure to 1% CO_2 would yield a fall in BCECF 513/438 emission ratios while exposure to NH_4Cl would cause an increase in the ratio. Furthermore, the washout of CO_2 and NH_4Cl was expected to elicit reversals of the BCECF ratios. Indeed, these patterns of BCECF 513/438 emission ratio changes were observed consistently in control experiments (Fig. 1). Moreover, the washout of NH_4Cl was associated with a decrease (undershoot) in HR BCECF 513/438 emission ratios below baseline values, indicative of cellular acidification related to compensatory accumulation of H^+ equivalents during the phase of alkalisation. It was also expected that compensatory secretion of H^+ equivalents during the CO_2-induced intracellular acidification would be reflected by an increase in the BCECF 513/438 ratio above baseline upon return to normocapnic conditions. Interestingly, this phenomenon was observed in control (sham-injected) fish in half of the experiments only (see below; Figs 3 and 5). Hereafter, we refer to pHi changes rather than changes in the BCECF 513/438 emission ratios.

pHi regulation in zebrafish HR cells during and after CO_2-induced acidosis

Boron and De Weer (1976) described in detail the changes in pHi in squid giant axons exposed to 5% CO_2 and subsequently returned to normocapnia. The complex changes in pHi described by these authors and the accompanying cellular mechanisms have subsequently been applied to a multitude of cell types and species including fish gill cells (e.g. Pelster, 2004; Parks et al., 2007; Parks et al., 2010) and hepatocytes (e.g. Walsh, 1986). Three phases of pHi changes are typical of cells exposed to, and then removed from, enriched CO_2 solutions. First, a phase of rapid acidification occurs, reflecting the diffusive entry of CO_2 and its hydration to HCO_3^- and H^+. Second, a 'plateau phase' is observed, representing a slow increase in pHi despite the continued presence of CO_2 that results from compensatory secretion of H^+ equivalents via regulated pathways. A third phase accompanies the removal of CO_2, which consists of a rapid alkalisation that may overshoot baseline pHi

Journal of Experimental Biology (2020) 223, jeb212928. doi:10.1242/jeb.212928

values. The extent of the overshoot during the rapid re-equilibration of CO_2 reflects the quantity of H^+ equivalents accumulated during the plateau phase and thus can be used as an index of intracellular acid–base compensation. However, it is important to emphasise that an additional acidification phase of intracellular acid–base adjustment occurs simultaneously with the plateau phase and indeed may even obscure the plateau phase entirely. During this additional phase, the cell continues to acidify slowly after initial CO_2 entry owing to outwardly directed HCO_3^- movements, which serve to lower the intracellular partial pressure of CO_2 and thus fuel continued entry of CO_2 into the cell, derived from the extracellular dehydration of the exported HCO_3^- (the Jacobs–Stewart cycle; Jacobs and Stewart, 1942). Thus, the net change in pHi during the plateau phase represents the opposing consequences of any compensatory secretion of H^+ coupled with the continued entry of H^+ via the Jacobs–Stewart cycle. Thus, compensation of pHi during CO_2-induced acidosis will occur as long as net cellular H^+ export exceeds the re-entry of CO_2, a condition that is normally met owing to the relatively slow uncatalysed rate of extracellular HCO_3^- dehydration.

Given this theoretical framework, we opted to estimate the degree of intracellular acid–base compensation and thus assess the roles of CA17a, NHE3b and HA in pHi regulation by comparing the changes in relative pHi between sham/wild-type and morphant/knockout fish over different phases of each experiment.

The role of CA17a in regulating intracellular acidosis

The specific cytosolic CA isoform, CA17a, is expressed abundantly in zebrafish HR cells (Lin et al., 2008), where it is thought to catalyse the hydration reaction of CO_2 to yield H^+ and HCO_3^- (reviewed by Guh et al., 2015). H^+ derived from the catalysed hydration of CO_2 is thereby made available to provide substrate for Na^+/H^+ exchange via NHE3b and H^+ secretion via HA. In support of this model, the selective knockdown of CA17a caused a significant decline in H^+ extrusion (as measured by SIET) in zebrafish larvae at 4 dpf (Lin et al., 2008). However, the effects of CA knockdown on H^+ extrusion were relatively modest (~20%). The effect of CA17a knockdown on decreasing the magnitude of net H^+ extrusion was similar to the inhibitory effect of NHE3b knockdown (Shih et al., 2012) but much less than the large reduction in H^+ secretion associated with HA knockdown (Horng et al., 2007).

In the present study, the effects of CA17a knockdown on pHi regulation during respiratory acidosis were consistent with its role in aiding the provision of H^+ for NHE3b and HA. During exposure to CO_2, HR cell pHi did not stabilise as was in the case of control fish, but continued to decrease in the morphants, indicating that any compensatory secretion of H^+ was unable to match the continuing acidification arising from the Jacobs–Stewart cycle (Fig. 2B). Moreover, upon return to normocapnic conditions, the morphants exhibited a significant blunting of the cellular re-alkalisation phase (Fig. 2B,C). Ultimately, the difference in pHi between the morphants and sham fish at the conclusion of the experiment must reflect the reduced secretion of H^+ via NHE3b or HA linked to catalysed hydration of CO_2. Although HR cell pHi was lower in the fish experiencing CA knockdown, suggesting that H^+ levels may not be limiting, it is more likely that the H^+ concentration in apical and sub-apical micro domains is the critical factor in providing H^+ for apical NHE and H^+-ATPase. Thus, the knockdown of CA, which is known to be localised near the apical membrane of ionocytes (Rahim et al., 1988; Ito et al., 2013), is likely to reduce H^+ levels in the vicinity of NHE and H^+-ATPase despite the macro-level reduction in pHi. Furthermore, given that CA17a knockdown (Gilmour et al., 2009) or knockout (A. M. Zimmer and S. F. Perry, unpublished data) does not affect CO_2 excretion in zebrafish larvae at 2 and 4 dpf, respectively, it is improbable that differences in CO_2 excretion contributed to the changes in pHi during and after hypercapnia that were observed in the present study after CA knockdown.

Despite its presumed contribution to both NHE and H^+-ATPase activities, the effects of CA loss of function on pHi regulation during hypercapnia were smaller than the effects of NHE3b or H^+-ATPase loss of function alone. These results are consistent with the findings of Horng et al. (2007), who demonstrated that the effects of CA17a knockdown on decreasing the magnitude of net H^+ extrusion (as measured by SIET) were much less than the large reduction in H^+ secretion associated with HA knockdown. In contrast, however, the smaller effect of CA knockdown on pHi regulation compared with NHE3 knockdown was not observed for H^+ extrusion in a previous study (Shih et al., 2012). Given that NHE3b is an electroneutral exchanger that is dependent on favourable chemical gradients, one might have expected the effects of CA17a knockdown on pHi regulation to more closely resemble the effects of NHE3b knockdown compared with knockdown of H^+-ATPase, which is able to transport H^+ against sizeable gradients.

Linking CA activity to Na^+ uptake and H^+ secretion in zebrafish has not proven straightforward. Although CA17a is believed to function as part of a multi-component transport metabolon with NHE3b and Rhcgb (previously named Rhcg1) (Ito et al., 2013) and its knockdown reduces the accumulation of Na^+ in HR cells (Ito et al., 2013), other studies have reported a stimulation of Na^+ uptake with CA17a knockdown in larvae (Lin et al., 2008) or adults acclimated to soft water (Boisen et al., 2003). It is possible that discrepancies between the results of studies obtained from specific measurements on HR cells (e.g. Ito et al., 2013) and those based on whole larva measurements (e.g. Kumai and Perry, 2011) reflect the compensatory influences of alternative Na^+ uptake pathways in non HR cells that do not rely on CA activity (i.e. Na^+-Cl^- co-transport in NCC cells).

The role of NHE3b and HA in regulating intracellular acidosis

The results of the present study revealed a significant impact of both NHE3b knockdown and knockout on HR cell pHi regulation. Although the Na^+ and H^+ chemical gradients across the apical membrane of HR cells are inconsistent with the function of electroneutral Na^+/H^+ exchange (see Parks et al., 2008), it is nevertheless clear that NHE3b does in fact contribute to Na^+ uptake in zebrafish larvae even under highly unfavourable conditions of low external pH (Kumai et al., 2012) or low external [Na^+] (Shih et al., 2012). Despite the unfavourable macroscopic chemical gradients for Na^+/H^+ exchange, it has been proposed that favourable localised gradients across the apical membrane are created via close association of NHE3b with Rhcgb and CA17a (Kumai et al., 2012; Shih et al., 2012; Ito et al., 2013). Thus, as proposed by Wright and Wood (2009), the outward diffusive movement of NH_3 via Rhcgb and its subsequent protonation to NH_4^+ serves to create a localised alkaline environment immediately adjacent to the gill epithelium. The increased pH of the external boundary layer, when coupled with the localised production of H^+ from CO_2 via CA17a in the sub-apical region of HR cells, is thought to thermodynamically enable NHE3b-mediated Na^+/H^+ exchange.

Given the proposed model for Na^+/H^+ exchange, a possible explanation for the larger detrimental effect of NHE3b knockdown compared with H^+-ATPase knockdown on pHi regulation during respiratory acidosis is that during H^+-ATPase knockdown, the influx

of CO_2 into the HR cells and the subsequent hydration to H^+ and HCO_3^- resulted in a further increase in $[H^+]$ in the HR cells in the vicinity of NHE3b, thus enabling Na^+/H^+ exchange disproportionally over stimulation of the energy-consuming HA pathway during NHE3b knockdown. Further supporting this theory is the 'plateau' during CO_2-induced acidification that occurred significantly later in NHE3b and CA17a morphants, but not in HA morphants, when compared with shams. Regardless, all three morphant groups, including the HA morphants, displayed a significant decrease in pHi change throughout the entire experiment compared with the sham controls. Thus, while NHE3b might be the preferred pathway for H^+ extrusion during CO_2-induced acidosis, the ATP-driven H^+-ATPase still remains a critical component for the long-term recovery of pHi from intracellular acidosis in HR cells.

It is of interest that slightly different results were obtained using the NHE3b morphants versus knockouts. However, as discussed by Zimmer et al. (2019a,b), both approaches have pros and cons. For example, morpholino knockdown may yield incomplete elimination of the target protein as well as off-target effects (Kok et al., 2015). In contrast, CRISPR-Cas9 knockout may lead to the activation of secondary mechanisms that may compensate for the complete absence of the target gene, as observed in multiple organisms (El-Brolosy and Stainier, 2017). Within the context of the present study, the degree of acidosis and alkalosis, and also the time points at which the minimum/maximum pHi values were reached, were remarkably similar in the NHE3b morpholino knockdown (Fig. 3B,C) and the NHE3b CRISPR/Cas9 knockout (Fig. 4C,D) larvae. Surprisingly, the wild-type embryos displayed a greater extent of intracellular acidosis during the CO_2 perfusion phase (0.20±0.03; Fig. 4D) compared with the morpholino sham controls in all of the other experiments (0.07±0.02, Fig. 2C; 0.06±0.02, Fig. 3C; 0.08±0.01, Fig. 5D). This suggests that difference strains/lines of zebrafish may exhibit different osmoregulatory capacities, which has been observed in other zebrafish lines in our lab (A.M.Z., unpublished data).

pHi regulation in zebrafish HR cells during external NH_4^+-induced alkalosis

Intracellular alkalosis was induced in HR cells by exposing the larvae to 20 mmol l^{-1} NH_4Cl whereby NH_3 is expected to enter the HR cells via Rhcgb (Nakada et al., 2007). Given the high pKa of the NH_3–NH_4^+–H^+ equilibrium reaction (~9.1–9.25 at 28°C; Cameron and Heisler, 1983) relative to typical pHi values (6.8–7.6), NH_3 will combine with H^+ to form NH_4^+, thereby raising pHi (Boron and De Weer, 1976). Assuming a similar cause of intracellular alkalosis in zebrafish larvae HR cells during exposure to NH_4Cl, it was expected that one or both of the apical membrane H^+ extrusion pathways (NHE3b or HA) would be reduced to facilitate H^+ retention. Interestingly, all fish, regardless of treatment, displayed similar increases in pHi during exposure to 20 mmol l^{-1} NH_4Cl and, with the exception of the CA morphants, exhibited equivalent degrees of acidification upon washout of NH_4Cl. The fact that the CA17a morphants did not experience a pHi undershoot upon NH_4Cl removal suggests reduced compensatory accumulation of H^+ during the period of NH_4Cl exposure in the morphants. Because inhibition of the apical H^+ extrusion pathways did not affect pHi regulation during alkalosis or the ensuing acidosis with NH_4Cl washout, it suggests that CA17a is providing substrate for another acid–base transporter. Although the focus of the present study was on HR apical membrane H^+ extrusion pathways, HR cells also expresses a basolateral Cl^-/HCO_3^- anion exchanger (isoform AE1b; *slc4a1b*) (Lee et al., 2011). Thus, it is possible that the major route of compensatory H^+ accumulation during NH_4Cl exposure occurs via HCO_3^- excretion, in which case the effect of CA17a knockdown on pHi regulation could be explained by a reduced supply of HCO_3^- for Cl^-/HCO_3^- exchange. The involvement of basolateral anion exchangers in acid–base regulation was demonstrated in type A intercalated cells in mammalian kidneys (Wagner et al., 2006). Furthermore, studies on the spotted green pufferfish (*Tetraodon nigroviridis*) demonstrated that AE1 colocalises with CA (Tang and Lee, 2007). Thus, it is possible that the catalysed hydration of CO_2 is required to stimulate HCO_3^- excretion across the basolateral membrane via AE1b, which would explain why a significant decrease in post-NH_4Cl acidosis was observed only in CA17a morphants, but not in NHE3b or HA morphants.

Future directions

The *in vivo* ratiometric imaging technique is applicable to cells for which vital markers are available. Because mitochondrial vital stains cannot discriminate ionocyte subtypes, at this time, studies on specific zebrafish ionocyte sub-populations are restricted to HR cells. We anticipate that with the development of new vital cell markers and the creation of transgenic lines of zebrafish expressing ionocyte-specific green fluorescent protein, this new method can be used to conduct time-lapse imaging in other ionocyte cell types, such as NaR and NCC cells. In addition, it may be possible to use other ratiometric dyes to measure the concentration of other ions such as Ca^{2+} and Na^+ in intracellular environments, as was done recently using the non-ratiometric Na^+-sensitive dye CoroNa Green in *Galaxias maculatus* (Lee et al., 2016).

Acknowledgements

Much of the material (results, methods, discussion, etc.) in this paper is reproduced from the MSc thesis of Hong Meng Yew (University of Ottawa, 2019). We are grateful to Dr Junya Hiroi for providing us with a rainbow trout NHE3b polyclonal antibody.

Competing interests

The authors declare no competing or financial interests.

Author contributions

Conceptualization: H.M.Y., S.F.P.; Methodology: H.M.Y., A.M.Z., S.F.P.; Software: H.M.Y.; Validation: H.M.Y.; Formal analysis: H.M.Y., S.F.P.; Resources: S.F.P.; Writing - original draft: H.M.Y.; Writing - review & editing: H.M.Y., A.M.Z., S.F.P.; Supervision: S.F.P.; Project administration: S.F.P.; Funding acquisition: S.F.P.

Funding

This research was supported by Natural Sciences and Engineering Research Council (NSERC) grants to S.F.P. A.M.Z. was the recipient of an NSERC Postdoctoral Fellowship.

Supplementary information

Supplementary information available online at
http://jeb.biologists.org/lookup/doi/10.1242/jeb.212928.supplemental

References

Abbas, L., Hajihashemi, S., Stead, L. F., Cooper, G. J., Ware, T. L., Munsey, T. S., Whitfield, T. T. and White, S. J. (2011). Functional and developmental expression of a zebrafish Kir1.1 (ROMK) potassium channel homologue Kcnj1. *J. Physiol.* **589**, 1489-1503. doi:10.1113/jphysiol.2010.200295

Bayaa, M., Vulesevic, B., Esbaugh, A., Braun, M., Ekker, M. E., Grosell, M. and Perry, S. F. (2009). The involvement of SLC26 anion transporters in chloride uptake in zebrafish (*Danio rerio*) larvae. *J. Exp. Biol.* **212**, 3283-3295. doi:10.1242/jeb.033910

Boisen, A. M. Z., Amstrup, J., Novak, I. and Grosell, M. (2003). Sodium and chloride transport in soft water and hard water acclimated zebrafish (*Danio rerio*). *Biochim. Biophys. Acta* **1618**, 207-218. doi:10.1016/j.bbamem.2003.08.016

Boron, W. F. and De Weer, P. (1976). Intracellular pH transients in squid giant axons caused by CO_2, NH_3, and metabolic inhibitors. *J. Gen. Physiol.* **67**, 91-112. doi:10.1085/jgp.67.1.91

Boyarsky, G., Hanssen, C. and Clyne, L. A. (1996). Superiority of in vitro over in vivo calibrations of BCECF in vascular smooth muscle cells. *FASEB J.* **10**, 1205-1212. doi:10.1096/fasebj.10.10.8751723

Cameron, J. N. and Heisler, N. (1983). Studies of ammonia in the rainbow trout: physico-chemical parameters, acid-base behaviour and respiratory clearance. *J. Exp. Biol.* **105**, 107-125.

Dymowska, A. K., Hwang, P.-P. and Goss, G. G. (2012). Structure and function of ionocytes in the freshwater fish gill. *Respir. Physiol. Neurobiol.* **184**, 282-292. doi:10.1016/j.resp.2012.08.025

El-Brolosy, M. A. and Stainier, D. Y. R. (2017). Genetic compensation: a phenomenon in search of mechanisms. *PLoS Genet.* **13**, e1006780. doi:10.1371/journal.pgen.1006780

Esaki, M., Hoshijima, K., Kobayashi, S., Fukuda, H., Kawakami, K. and Hirose, S. (2007). Visualization in zebrafish larvae of Na^+ uptake in mitochondria-rich cells whose differentiation is dependent on Foxi3a. *Am. J. Physiol. Regul. Integr. Comp. Physiol.* **292**, R470-R480. doi:10.1152/ajpregu.00200.2006

Esbaugh, A. J., Perry, S. F., Bayaa, M., Georgalis, T., Nickerson, J., Tufts, B. L. and Gilmour, K. M. (2005). Cytoplasmic carbonic anhydrase isozymes in rainbow trout *Oncorhynchus mykiss*: comparative physiology and molecular evolution. *J. Exp. Biol.* **208**, 1951-1961. doi:10.1242/jeb.01551

Evans, D. H., Piermarini, P. M. and Choe, K. P. (2005). The multifunctional fish gill: dominant site of gas exchange, osmoregulation, acid-base regulation, and excretion of nitrogenous waste. *Physiol. Rev.* **85**, 97-177. doi:10.1152/physrev.00050.2003

Ferreira-Martins, D., McCormick, S. D., Campos, A., Lopes-Marques, M., Osório, H., Coimbra, J., Castro, L. F. C. and Wilson, J. M. (2016). A cytosolic carbonic anhydrase molecular switch occurs in the gills of metamorphic sea lamprey. *Sci. Rep.* **6**, 33954. doi:10.1038/srep33954

Gilmour, K. M. and Perry, S. F. (2009). Carbonic anhydrase and acid-base regulation in fish. *J. Exp. Biol.* **212**, 1647-1661. doi:10.1242/jeb.029181

Gilmour, K. M., Thomas, K., Esbaugh, A. J. and Perry, S. F. (2009). Carbonic anhydrase expression and CO_2 excretion during early development in zebrafish *Danio rerio*. *J. Exp. Biol.* **212**, 3837-3845. doi:10.1242/jeb.034116

Graber, M. L., DiLillo, D. C., Friedman, B. L. and Pastoriza-Munoz, E. (1986). Characteristics of fluoroprobes for measuring intracellular pH. *Anal. Biochem.* **156**, 202-212. doi:10.1016/0003-2697(86)90174-0

Guh, Y.-J., Lin, C.-H. and Hwang, P.-P. (2015). Osmoregulation in zebrafish: ion transport mechanisms and functional regulation. *EXCLI J.* **14**, 627-659.

Hiroi, J. and McCormick, S. D. (2012). New insights into gill ionocyte and ion transporter function in euryhaline and diadromous fish. *Respir. Physiol. Neurobiol.* **184**, 257-268. doi:10.1016/j.resp.2012.07.019

Horng, J.-L., Lin, L.-Y., Huang, C.-J., Katoh, F., Kaneko, T. and Hwang, P.-P. (2007). Knockdown of V-ATPase subunit A (*atp6v1a*) impairs acid secretion and ion balance in zebrafish (*Danio rerio*). *Am. J. Physiol. Regul. Integr. Comp. Physiol.* **292**, R2068-R2076. doi:10.1152/ajpregu.00578.2006

Hwang, P.-P. (2009). Ion uptake and acid secretion in zebrafish (*Danio rerio*). *J. Exp. Biol.* **212**, 1745-1752. doi:10.1242/jeb.026054

Hwang, P.-P. and Chou, M.-Y. (2013). Zebrafish as an animal model to study ion homeostasis. *Pflugers Arch.* **465**, 1233-1247. doi:10.1007/s00424-013-1269-1

Hwang, P.-P. and Perry, S. F. (2010). 8-Ionic and acid–base regulation. *Fish Physiol.* **29**, 311-344. doi:10.1016/S1546-5098(10)02908-0

Hwang, P.-P., Lee, T.-H. and Lin, L.-Y. (2011). Ion regulation in fish gills: recent progress in the cellular and molecular mechanisms. *Am. J. Physiol. Regul. Integr. Comp. Physiol.* **301**, R28-R47. doi:10.1152/ajpregu.00047.2011

Ito, Y., Kobayashi, S., Nakamura, N., Miyagi, H., Esaki, M., Hoshijima, K. and Hirose, S. (2013). Close association of carbonic anhydrase (CA2a and CA15a), Na^+/H^+ exchanger (Nhe3b), and ammonia transporter Rhcg1 in zebrafish ionocytes responsible for Na^+ uptake. *Front. Physiol.* **4**, 59. doi:10.3389/fphys.2013.00059

Jacobs, M. H. and Stewart, D. R. (1942). The role of carbonic anhydrase in certain ionic exchanges involving the erythrocyte. *J. Gen. Physiol.* **25**, 539-552. doi:10.1085/jgp.25.4.539

James-Kracke, M. R. (1992). Quick and accurate method to convert BCECF fluorescence to pHi: calibration in three different types of cell preparations. *J. Cell. Physiol.* **151**, 596-603. doi:10.1002/jcp.1041510320

Jao, L.-E., Wente, S. R. and Chen, W. (2013). Efficient multiplex biallelic zebrafish genome editing using a CRISPR nuclease system. *Proc. Natl. Acad. Sci. USA* **110**, 13904-13909. doi:10.1073/pnas.1308335110

Kok, F. O., Shin, M., Ni, C.-W., Gupta, A., Grosse, A. S., van Impel, A., Kirchmaier, B. C., Peterson-Maduro, J., Kourkoulis, G., Male, I. et al. (2015). Reverse genetic screening reveals poor correlation between morpholino-induced and mutant phenotypes in zebrafish. *Dev. Cell* **32**, 97-108. doi:10.1016/j.devcel.2014.11.018

Kumai, Y. and Perry, S. F. (2011). Ammonia excretion via Rhcg1 facilitates Na^+ uptake in larval zebrafish, *Danio rerio*, in acidic water. *Am. J. Physiol. Regul. Integr. Comp. Physiol.* **301**, R1517-R1528. doi:10.1152/ajpregu.00282.2011

Kumai, Y. and Perry, S. F. (2012). Mechanisms and regulation of Na^+ uptake by freshwater fish. *Respir. Physiol. Neurobiol.* **184**, 249-256. doi:10.1016/j.resp.2012.06.009

Kumai, Y., Nesan, D., Vijayan, M. M. and Perry, S. F. (2012). Cortisol regulates Na^+ uptake in zebrafish, *Danio rerio*, larvae via the glucocorticoid receptor. *Mol. Cell. Endocrinol.* **364**, 113-125. doi:10.1016/j.mce.2012.08.017

Kumai, Y., Porteus, C. S., Kwong, R. W. M. and Perry, S. F. (2015). Hydrogen sulfide inhibits Na^+ uptake in larval zebrafish, *Danio rerio*. *Pflugers Arch.* **467**, 651-664. doi:10.1007/s00424-014-1550-y

Kwong, R. W. M., Kumai, Y. and Perry, S. F. (2014). The physiology of fish at low pH: the zebrafish as a model system. *J. Exp. Biol.* **217**, 651-662. doi:10.1242/jeb.091603

Labun, K., Montague, T. G., Gagnon, J. A., Thyme, S. B. and Valen, E. (2016). CHOPCHOP v2: a web tool for the next generation of CRISPR genome engineering. *Nucleic Acids Res.* **44**, W272-W276. doi:10.1093/nar/gkw398

Lee, Y.-C., Yan, J.-J., Cruz, S. A., Horng, J.-L. and Hwang, P.-P. (2011). Anion exchanger 1b, but not sodium-bicarbonate cotransporter 1b, plays a role in transport functions of zebrafish H^+-ATPase-rich cells. *Am. J. Physiol. Cell Physiol.* **300**, C295-C307. doi:10.1152/ajpcell.00263.2010

Lee, J. A., Collings, D. A. and Glover, C. N. (2016). A model system using confocal fluorescence microscopy for examining real-time intracellular sodium ion regulation. *Anal. Biochem.* **507**, 40-46. doi:10.1016/j.ab.2016.05.008

Liao, B.-K., Deng, A.-N., Chen, S.-C., Chou, M.-Y. and Hwang, P.-P. (2007). Expression and water calcium dependence of calcium transporter isoforms in zebrafish gill mitochondrion-rich cells. *BMC Genomics* **8**, 354. doi:10.1186/1471-2164-8-354

Lin, L.-Y., Horng, J.-L., Kunkel, J. G. and Hwang, P.-P. (2006). Proton pump-rich cell secretes acid in skin of zebrafish larvae. *Am. J. Physiol. Cell Physiol.* **290**, C371-C378. doi:10.1152/ajpcell.00281.2005

Lin, T.-Y., Liao, B.-K., Horng, J.-L., Yan, J.-J., Hsiao, C.-D. and Hwang, P.-P. (2008). Carbonic anhydrase 2-like a and 15a are involved in acid-base regulation and Na^+ uptake in zebrafish H^+-ATPase-rich cells. *Am. J. Physiol. Cell Physiol.* **294**, C1250-C1260. doi:10.1152/ajpcell.00021.2008

Marshall, W. S. and Grosell, M. (2006). Ion transport, osmoregulation, and acid-base balance. *Physiol. Fish.* **3**, 177-230.

Miller, S., Pollack, J., Bradshaw, J., Kumai, Y. and Perry, S. F. (2014). Cardiac responses to hypercapnia in larval zebrafish (*Danio rerio*): the links between CO_2 chemoreception, catecholamines and carbonic anhydrase. *J. Exp. Biol.* **217**, 3569-3578. doi:10.1242/jeb.107987

Molich, A. and Heisler, N. (2005). Determination of pH by microfluorometry: intracellular and interstitial pH regulation in developing early-stage fish embryos (*Danio rerio*). *J. Exp. Biol.* **208**, 4137-4149. doi:10.1242/jeb.01878

Montague, T. G., Cruz, J. M., Gagnon, J. A., Church, G. M. and Valen, E. (2014). CHOPCHOP: a CRISPR/Cas9 and TALEN web tool for genome editing. *Nucleic Acids Res.* **42**, W401-W407. doi:10.1093/nar/gku410

Montrose, M. H. and Murer, H. (1986). Regulation of intracellular pH in LLC-PK1 cells by Na^+/H^+ exchange. *J. Membr. Biol.* **93**, 33-42. doi:10.1007/BF01871016

Nakada, T., Hoshijima, K., Esaki, M., Nagayoshi, S., Kawakami, K. and Hirose, S. (2007). Localization of ammonia transporter Rhcg1 in mitochondrion-rich cells of yolk sac, gill, and kidney of zebrafish and its ionic strength-dependent expression. *Am. J. Physiol. Regul. Integr. Comp. Physiol.* **293**, R1743-R1753. doi:10.1152/ajpregu.00248.2007

Parks, S. K., Tresguerres, M. and Goss, G. G. (2007). Interactions between Na^+ channels and Na^+-HCO_3^- cotransporters in the freshwater fish gill MR cell: a model for transepithelial Na^+ uptake. *Am. J. Physiol. Cell Physiol.* **292**, C935-C944. doi:10.1152/ajpcell.00604.2005

Parks, S. K., Tresguerres, M. and Goss, G. G. (2008). Theoretical considerations underlying Na^+ uptake mechanisms in freshwater fishes. *Comp. Biochem. Physiol. C. Toxicol. Pharmacol.* **148**, 411-418. doi:10.1016/j.cbpc.2008.03.002

Parks, S. K., Tresguerres, M., Galvez, F. and Goss, G. G. (2010). Intracellular pH regulation in isolated trout gill mitochondrion-rich (MR) cell subtypes: evidence for Na^+/H^+ activity. *Comp. Biochem. Physiol. A. Mol. Integr. Physiol.* **155**, 139-145. doi:10.1016/j.cbpa.2009.10.025

Pelster, B. (2004). pH regulation and swimbladder function in fish. *Respir. Physiol. Neurobiol.* **144**, 179-190. doi:10.1016/j.resp.2004.03.019

Perry, S. F., Vulesevic, B., Grosell, M. and Bayaa, M. (2009). Evidence that SLC26 anion transporters mediate branchial chloride uptake in adult zebrafish (*Danio rerio*). *Am. J. Physiol. Regul. Integr. Comp. Physiol.* **297**, R988-R997. doi:10.1152/ajpregu.00327.2009

Rahim, S. M., Delaunoy, J.-P. and Laurent, P. (1988). Identification and immunocytochemical localization of two different carbonic anhydrase isoenzymes in teleostean fish erythrocytes and gill epithelia. *Histochemistry* **89**, 451-459. doi:10.1007/BF00492602

Shih, T.-H., Horng, J.-L., Hwang, P.-P. and Lin, L.-Y. (2008). Ammonia excretion by the skin of zebrafish (*Danio rerio*) larvae. *Am. J. Physiol. Cell Physiol.* **295**, C1625-C1632. doi:10.1152/ajpcell.00255.2008

Shih, T.-H., Horng, J.-L., Liu, S.-T., Hwang, P.-P. and Lin, L.-Y. (2012). Rhcg1 and NHE3b are involved in ammonium-dependent sodium uptake by zebrafish larvae acclimated to low-sodium water. *Am. J. Physiol. Regul. Integr. Comp. Physiol.* **302**, R84-R93. doi:10.1152/ajpregu.00318.2011

Takeyasu, K., Tamkun, M. M., Renaud, K. J. and Fambrough, D. M. (1988). Ouabain-sensitive (Na^+/K^+)-ATPase activity expressed in mouse L cells by

transfection with DNA encoding the alpha-subunit of an avian sodium pump. *J. Biol. Chem.* **263**, 4347-4354.

Talbot, J. C. and Amacher, S. L. (2014). A streamlined CRISPR pipeline to reliably generate zebrafish frameshifting alleles. *Zebrafish* **11**, 583-585. doi:10.1089/zeb.2014.1047

Tang, C. H. and Lee, T. H. (2007). The novel correlation of carbonic anhydrase II and anion exchanger 1 in gills of the spotted green pufferfish, *Tetraodon nigroviridis*. *J. Exp. Zool. A. Ecol. Genet. Physiol.* **307**, 411-418. doi:10.1002/jez.391

Ura, K., Soyano, K., Omoto, N., Adachi, S. and Yamauchi, K. (1996). Localization of Na^+,K^+-ATPase in tissues of rabbit and teleosts using an antiserum directed against a partial sequence of the α-subunit. *Zoolog. Sci.* **13**, 219-227. doi:10.2108/zsj.13.219

Varsamos, S., Nebel, C. and Charmantier, G. (2005). Ontogeny of osmoregulation in postembryonic fish: a review. *Comp. Biochem. Physiol. A Mol. Integr. Physiol.* **141**, 401-429. doi:10.1016/j.cbpb.2005.01.013

Wagner, C. A., Kovacikova, J., Stehberger, P. A., Winter, C., Benabbas, C. and Mohebbi, N. (2006). Renal acid-base transport: old and new players. *Nephron. Physiol.* **103**, p1-p6. doi:10.1159/000090217

Walsh, P. J. (1986). Ionic requirements for intracellular pH regulation in rainbow trout hepatocytes. *Am. J. Physiol.* **250**, R24-R29. doi:10.1152/ajpregu.1986.250.1.R24

Wang, Y.-F., Tseng, Y.-C., Yan, J.-J., Hiroi, J. and Hwang, P.-P. (2009). Role of SLC12A10.2, a Na-Cl cotransporter-like protein, in a Cl uptake mechanism in zebrafish (*Danio rerio*). *Am. J. Physiol. Regul. Integr. Comp. Physiol.* **296**, R1650-R1660. doi:10.1152/ajpregu.00119.2009

Westerfield, M. (1995). *The Zebrafish Book: A Guide for the Laboratory use of Zebrafish (Brachydanio rerio)*. University of Oregon Press.

Wright, P. A. and Wood, C. M. (2009). A new paradigm for ammonia excretion in aquatic animals: role of Rhesus (Rh) glycoproteins. *J. Exp. Biol.* **212**, 2303-2312. doi:10.1242/jeb.023085

Yan, J.-J., Chou, M.-Y., Kaneko, T. and Hwang, P.-P. (2007). Gene expression of Na^+/H^+ exchanger in zebrafish H^+-ATPase-rich cells during acclimation to low-Na^+ and acidic environments. *Am. J. Physiol. Cell Physiol.* **293**, C1814-C1823. doi:10.1152/ajpcell.00358.2007

Zimmer, A. M., Do, J., Szederkenyi, K., Chen, A., Morgan, A. L. R., Jensen, G., Pan, Y. K., Gilmour, K. M. and Perry, S. F. (2019a). Use of gene knockout to examine serotonergic control of ion uptake in zebrafish reveals the importance of controlling for genetic background: a cautionary tale. *Comp. Biochem. Physiol. A Mol. Integr. Physiol.* **238**, 110558. doi:10.1016/j.cbpa.2019.110558

Zimmer, A. M., Pan, Y. K., Chandrapalan, T., Kwong, R. W. M. and Perry, S. F. (2019b). Loss-of-function approaches in comparative physiology: is there a future for knockdown experiments in the era of genome editing? *J. Exp. Biol.* **222**, jeb175737. doi:10.1242/jeb.175737

Zimmer, A. M., Shir-Mohammadi, K., Kwong, R. W. M. and Perry, S. F. (2020). Reassessing the contribution of the Na^+/H^+ exchanger Nhe3b to Na^+ uptake in zebrafish (*Danio rerio*) using CRISPR/Cas9 gene editing. *J. Exp. Biol.* **223**, jeb215111. doi:10.1242/jeb.215111

Supplementary Figures

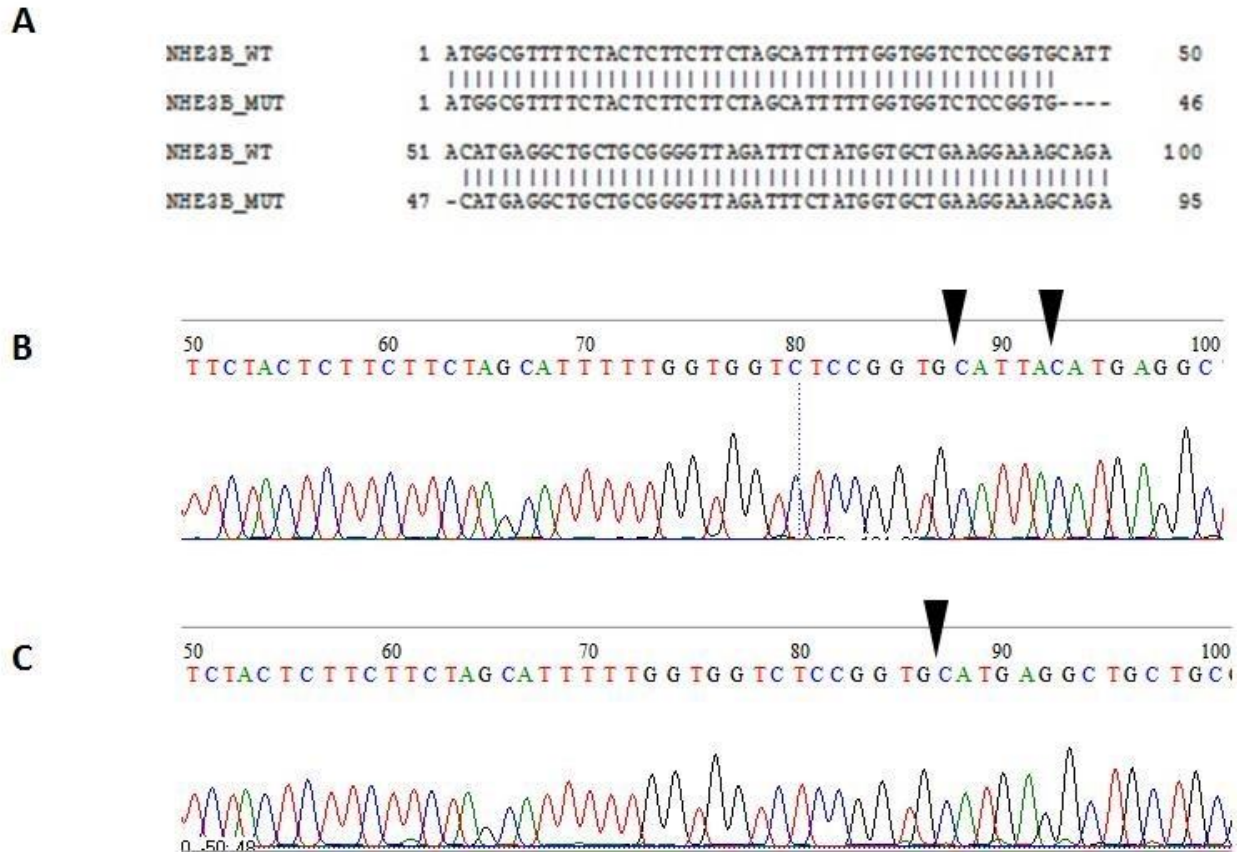

Figure S1. DNA sequence of a deletion mutation of the NHE3b transcript in zebrafish used in the study generated using the CRISPR-Cas9 gene editing technique. Sequence alignment of wildtype .and mutant genotypes displays a 5bp deletion in the mutants near the N-terminal of the transcript, between base pairs 46 - 51 of the wild-type transcript (A). Sanger sequencing data of DNA digests obtained from adult fin clips display the base pair differences between the wildtype (B) and mutant (C) genotypes, as indicated by black arrows.

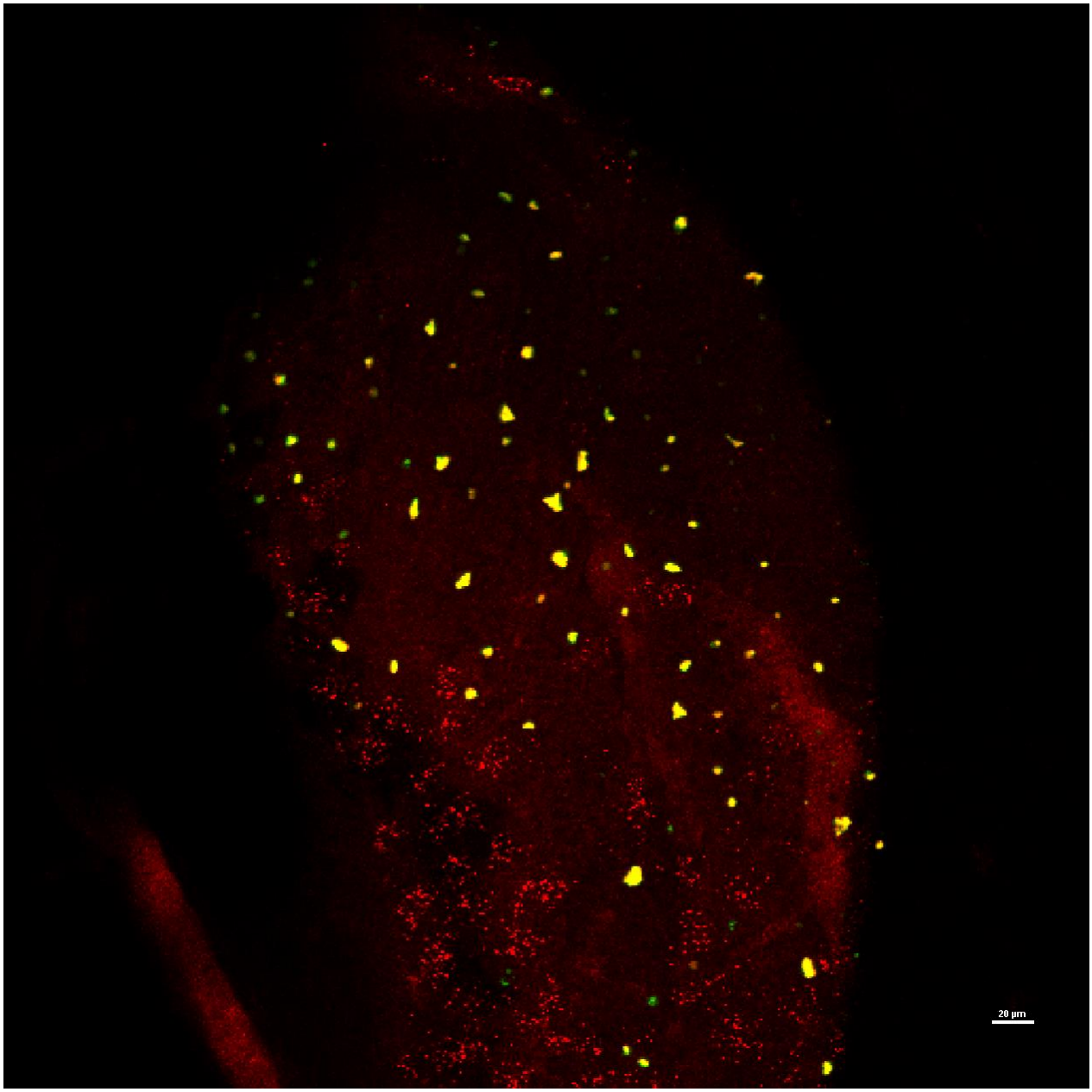

Figure S2. Representative whole mount immunohistochemistry images indicating the presence of (A) NHE3b (red) or (B) concanavalin A (ConA; green) in yolk sac epithelium of wild-type zebrafish (*Danio rerio*) larva at 4 dpf. The merged image (C) illustrates that NHE3b is co-localised to ConA positive cells indicating that these cells are HR cell ionocytes. A small percentage of ConA positive cells did not exhibit NHE3b staining. The scale bar represent 20 µM.

Methods**.** Larvae were exposed for 25 min to Concanavalin A (ConA) Alexa Fluor 633 conjugate (50 mg/ml), killed with anaesthetic overdose (MS-222) and fixed for 45 min with 4% PFA in PBS

(pH 7.3). After washing with PBS-T, specimens were blocked for 1 h using 3% BSA/PBS-T and then incubated with an affinity purified rabbit polyclonal antibody (1:200 dilution) raised against a cocktail of synthetic peptides corresponding to two regions of rainbow trout NHE3b (position 755–769: GDEDFEFSEGDSASG; 818–839: PSQRAQLRLPWTPSNLRRLAPL**)** (Zimmer et al., 2016). The longer of the two antigenic peptides shares 91% (19/21) amino acid identity with the corresponding zebrafish sequence. Subsequent washing, application of secondary antibody and microscopic imaging were performed as described in Materials and Methods.